THE EFFECT OF GRAIN VOLUME DISTRIBUTION ON THE MECHANICAL PROPERTIES OF HIGH PURITY ALUMINUM

By

ATUL B. GOKHALE

A DISSERTATION PRESENTED TO THE GRADUATE SCHOOL
OF THE UNIVERSITY OF FLORIDA IN PARTIAL FULFILLMENT
OF THE REQUIREMENTS FOR THE DEGREE OF
DOCTOR OF PHILOSOPHY

UNIVERSITY OF FLORIDA

1995

UNIVERSITY OF FLORIDA LIBRARIES

Copyright 1995

By

Atul B. Gokhale

Dedicated to my wife, Jayoo
whose patience finally ran out

and

To my parents, Balkrishna and Leela Gokhale

ACKNOWLEDGEMENTS

I would first and foremost like to express my deep gratitude to late Prof. Frederick N. Rhines under whose guidance this work was completed. It was his hypothesis which formed the basis for this work, and his great spirit, integrity and support which kept me going. I would also like to extend my sincere thanks to my committee, Profs. Robert T. DeHoff, Reza Abbaschian, Robert E. Reed-Hill, Richard G. Connell, Jr. and Robert L. Scheaffer. Special thanks are also due to my numerous colleagues who gave me constant support and encouragement during the course of this work.

TABLE OF CONTENTS

page

ACKNOWLEDGEMENTS....................iv

ABSTRACT....................viii

CHAPTERS

1. INTRODUCTION....................1

2. THE GRAIN SIZE DISTRIBUTION....................4

   2.1 Introduction....................4

   2.2 Experimental Methods....................9

   2.2.1 Material....................9
   2.2.2 Thermomechanical Treatments....................11

   2.3 Determination of the Grain Volume Distribution....................14

   2.3.1 Embrittlement Characteristics....................14
   2.3.2 Embrittlement and Separation Procedure....................16
   2.3.3 Separation Efficiency and Metal Loss....................22

   2.4 Results....................25

   2.4.1 Tests of Lognormality....................31
   2.4.2 Data Analysis....................32
   2.4.3 Effect of Strain Prior to Recrystallization....................34
   2.4.4 Transformation of the Variable....................41

   2.5 Genesis of the Lognormal Distribution....................42

   2.5.1 Evolution During Recrystallization....................43
   2.5.2 Cell Area Calculations....................45

2.5.3 Constancy of the Grain Volume Distribution Width........................46

3. MECHANICAL BEHAVIOR OF ALUMINUM POLYCRYSTALS......49

3.1 Introduction..49

3.1.1 Analytical Approach..52
3.1.2 Dislocation Approach...58
3.1.2.1 Dislocation pileup approach..58
3.1.2.2 Non-pileup approach...63
3.1.3 Size Distribution Approach...67
3.1.4 Summary of Aluminum Tensile Properties......................................74

3.2 Experimental Procedure...79

3.3 Results and Discussion...88

3.3.1 Background...89
3.3.1.1 True stress and true strain...89
3.3.1.2 The yield strength..90
3.3.1.3 Stress at uniform strain limit...91
3.3.1.4 True fracture strain...92
3.3.2 Results...92
3.3.2.1 The yield behavior...92
3.3.2.2 Post yield flow behavior...104
3.3.2.3 Stress at instability, maximum uniform strain
and fracture strain...131

4. DISCUSSION...139

4.1 Progression of Plastic Deformation in Polycrystals...........................139

4.2 Microyield...141

4.2.1 Elastic Incompatibility...141
4.2.2 Onset of Microyielding..142

4.3 Macroyielding...144

4.3.1 Connection to the Grain Volume Distribution................................147

4.4 Strain Hardening...153

4.5 Neck Formation..156

5. CONCLUSIONS AND FUTURE WORK 158

5.1 Conclusions 158

5.2 Future Work 159

REFERENCES 161

BIOGRAPHICAL SKETCH 169

Abstract of Dissertation Presented to the Graduate School
of the University of Florida in Partial Fulfillment of the
Requirements for the Degree of Doctor of Philosophy

THE EFFECT OF GRAIN VOLUME DISTRIBUTION ON THE MECHANICAL PROPERTIES OF HIGH PURITY ALUMINUM

By

Atul B. Gokhale
December, 1995

Chairman: R.T. DeHoff
Major Department: Materials Science and Engineering

The plastic response of high purity aluminum polycrystals was found to depend strongly on the dispersion in grain volumes, quantified by determining their distribution via a grain separation technique. The distributions so determined were consistently well approximated as lognormal, whose parameters could be systematically altered by controlling the thermomechanical history of the samples. In particular, the evolution of the width of the lognormal distribution function, $\ln\sigma_g$, was found to depend strongly on the absolute as well as the relative severities of deformation steps of the deformation/recrystallization sequence. For all deformation histories, however, $\ln\sigma_g$ decreased monotonically in a power law manner with increasing severity of the final deformation step. In addition, it was found that the $\ln\sigma_g$ attained in the final recrystallization step remained constant during subsequent grain growth.

Using a strategy which combined thermomechanical treatments and isothermal annealing, a series of samples were produced with desired $\ln\sigma_g$ levels but nominally the same average grain boundary area per unit volume (S_v). Samples with two levels of S_v (8 and 4.45 mm^2/mm^3) and $\ln\sigma_g$'s ranging from 1.01 to 2.78 were used. The mechanical behavior of these polycrystals, tested at 77 K in uniaxial tension, indicated that $\ln\sigma_g$ exerted a significant control over the plastic response. In particular, the yield strength, work hardening rate and uniform elongation decreased monotonically with increasing $\ln\sigma_g$, the yield strength and work hardening rate being strongly linearly dependent on $(\ln\sigma_g)^{-2}$. Based on these observations, a view of polycrystalline deformation which considers strain gradients on the scale of grain size and domination of the plastic response by the largest grains in the microstructure is presented. Finally, microstructure based calculations are developed which show that the yield strength can be predicted by using a grain volume distribution dependent Hall-Petch mechanism.

CHAPTER 1

INTRODUCTION

This is a fundamental metallurgical investigation on the mechanical behavior of single phase polycrystals, based on an hypothesis first put forth by Prof. F.N. Rhines in the late 1970's. He suggested that the dispersion in the individual grain sizes (volumes) inherent to all polycrystals may have an effect on their plastic response.

It has long been recognized that a variation in grain sizes is a common feature of all polycrystalline materials. However, the quantification of this property is not straightforward. One may, for example, readily observe a variation in the sizes of grains via classical metallographic techniques. This type of single microsection, two-dimensional examination (which may be assumed to occur in more than 99% of the cases) can not however be used to estimate the true grain size (and therefore the dispersion in grain sizes) because: (1) a random section through an hypothetical polycrystal comprised of grains of *equal* size would nevertheless exhibit a variation in the grain areas, (2) on a random section through a real polycrystal, the probability of sectioning a grain is greater, the bigger it is, leading to an overestimation of larger grains and (3) the curvature of the grain faces.[1]

---

[1] These factors are discussed in greater detail in subsequent chapters.

In order to test the Rhines hypothesis, the first task then was to measure the three dimensional grain sizes unambiguously and quantify the grain size distribution. The second task was to test the effect of grain size variation while minimizing the effect of other microstructural features, most notably that of the average grain boundary area per unit volume in the polycrystal.

The first task, i.e. the determination of the grain volume distribution, was greatly simplified due to the excellent earlier work of Patterson [78Pat]. He used grain separation of as-cast and thermomechanically treated aluminum polycrystals to determine the grain volume distribution, and showed that the volume distribution could be well approximated as lognormal. He also showed that the degree of dispersion of grain volumes (quantified by the grain volume distribution width) could be controlled by thermomechanical treatments and remained constant during steady state grain growth.

In the present investigation, the control of the grain volume distribution width via thermomechanical treatments was explored further. The constancy of the grain volume distribution width during steady state grain growth was also confirmed. Using this information, a schedule of thermomechanical treatments and isothermal annealing was devised to obtain a desired combination of the grain volume distribution width and grain boundary area per unit volume. The aluminum polycrystals, which were characterized in terms of both the three dimensional grain volume (weight) distribution and the grain boundary area per unit volume, were tested in uniaxial tension.

The main contribution of this investigation is to show, for the first time, that the grain volume distribution width exerts a significant degree of control over the plastic response of aluminum polycrystals. It will be shown that all aspects of aluminum polycrystal plasticity, from yield to fracture, are affected by the grain volume distribution width.

The experimental results and microstructure-property correlations are presented in the next three chapters, along with a survey of the pertinent literature. Chapter 2 deals with the determination of the grain volume distribution width, while chapter 3 deals with the mechanical behavior of the polycrystals. A discussion on the connection between the grain volume distribution and the mechanical behavior of polycrystals is presented in chapter 4, which also includes microstructure-based calculations for the prediction of yield.

CHAPTER 2

THE GRAIN SIZE DISTRIBUTION

2.1 Introduction

Examination of a two-dimensional section through a polycrystal reveals grains of varying sizes. This variation can be ascribed to two factors, which are: (1) the position at which a particular grain may happen to be sectioned and (2) a variation in the sizes of the grains themselves. These two factors, together with a variation in grain shapes, make it impossible to assign an unambiguous size value through the measurement of either areas or intercept lengths to any specific grains in the polycrystal thus examined.

In spite of this objection, several studies have been reported which characterize the microstructure on the basis of either grain area distributions [57Fel, 68Sch] or grain intercept length distributions [68Hen, 68Sch, 79Gan, 80Fra]. In all cases, the distributions are well approximated as log-normal.[1] The interest in these distributions based on two-dimensional measurements is understandable for two reasons: (1) although indirect, there must be a relationship between the three dimensional distribution and the distributions generated from a random two-dimensional section. For example, if the range of three dimensional sizes increases, so must that deduced from the two-dimensional section (though the two are not simply related) and (2) the determination of the three dimensional distribution is much more tedious.

---

[1] With the exception of ferritic steel [68Sch, 71Abr] and α-iron [84Liu]. The origin and properties of the log-normal distribution are discussed later in this chapter.

Instances where a three-dimensional characterization of the microstructure has been carried out are rare in the literature. The method most frequently used has been serial sectioning, where successive microsectioning and superimposition of the two-dimensional section micrographs allows one to get at the third dimension [63Pos, 65Dye, 65Hop, 72Oka, 75Eig, 76Rhi, 78Pat, 83Wat, 84Liu].

Other methods include microradiography, magnetic domain transitions and grain separation. Microradiography was used by Williams and Smith [52Wil] to examine an Al-Sn alloy in three dimensions, deducting the size distribution through a comparison between the radiographic image and spheres of known volume. Otala [74Ota] and Otala and Sanagakangas [72Ota] used a non-destructive electromagnetic analyzer for studying ferrous alloys. The method is based on the statistical behavior of the magnetic domain transitions, brought about by an external magnetic field which varies at a suitable rate, the transitions being statistically related to the grain volumes. A refinement of the technique was used by Liu [84Liu] for pure iron, performing the analysis on a structure calibrated through serial sectioning. The method is, however, restricted to ferromagnetic materials.

In the present investigation, the method of separation of a polycrystal into its component grains by liquid metal embrittlement has been used to determine the grain volume distribution. This method is perhaps the most direct and least tedious of all those used for the purpose. Its use is, however, restricted by the availability of a suitable embrittlement couple (i.e. a solid-liquid metal combination) through which complete grain boundary penetration and embrittlement can be achieved. In the case of aluminum, gallium satisfies this requirement. The technique was first used by Patterson [78Pat, 82Rhi1] to study the topology and size distribution of grains in aluminum and the procedure described in this chapter is a refinement of this technique [82Rhi1].

It will be shown that the distribution of grain weights is consistently well approximated as log-normal. It will be further shown that the distribution width can be systematically controlled by controlling the deformation history of the samples. Both these findings support an earlier study by Rhines and Patterson [82Rhi2] on pure aluminum, where the grain volume distributions were shown to be log-normal, and the distribution width was shown to vary monotonically with the degree of deformation prior to recrystallization and annealing. In the present study, the effect of deformation has been extended to include the pre-final step deformation.

The history of the log-normal distribution, though not as old as the normal and Poisson distributions, can be traced as far back as 1879. McAlister [1879Mca] first set down the theory of the distribution in some detail in that year. Since then, a log-normal distribution of the variable has been observed to occur in a wide variety of systems. In the examples listed in Table 2.1, chosen because of the diversity of phenomena they represent, the distribution was well approximated as log-normal.

In light of the above, it is perhaps not surprising that other natural systems, particularly the distribution of grain volumes in recrystallized metals should also be log-normal. The underlying mechanisms through which a log-normal distribution evolves is

Table 2.1
Examples of a wide variety of systems exhibiting a lognormal distribution of the variable.

Hatch and Choate [29Hat]	Dust particles
Halmos [44Hal] and Epstein [47Eps]	Small particles evolved by a breakage or grinding process
Day [49Day]	Price changes over time for a large number of commodities
Higuchi and Hiestand [63Hig]	Particles in bio-pharmaceutics
Granqvist and Buhrman [76Gra]	Particles of precipitated noble metals
Joyce et al. [76Joy]	Lifetimes of solid state GaAlAs lasers
Skog [80Sko]	Alcohol consumption in humans
Franetoric et al. [80Fra]	Grains in splat cooled aluminum
Rhines et al. [82Rhi3]	Grain volumes in cast Al-Zn alloys
Palmer et al. [87Pal]	Grains in sputtered Ge thin films
Hoffmeister and Bayuzick [94Hof]	Bulk undercoolings in Zr

known to place some special constraints on the evolving system. For this reason, a brief discussion on the evolution of the log-normal distribution has been included with special reference to the behavior of a metal during recrystallization and subsequent grain growth.

Finally, the question may be asked: why the insistence on characterizing the structure in three dimensions when it is possible to characterize them as we "see" them, i.e., in two dimensions with much less effort. The answer may be given succinctly in the form of a quote from Rhines:[2]

> *The microstructures of all materials are three-dimensional in character and exist as multi-body networks in nature. Thus, any study which hopes to correlate the microstructures with their response to external stimuli must take the whole network into consideration. Whereas, the unitary two-dimensional approach may be temporarily satisfying and yield justifiable results, it must be ultimately discarded in favor of the more rigorous three-dimensional view.*

This viewpoint will be seen to be amply justified in the next chapter, where data relating the global grain volume distribution parameters to mechanical properties are presented. In this regard, it must be stressed that these microstructure-plastic response correlations do not, per se, require the grain volume distribution to be lognormal or indeed of any particular mathematical form. What is essential is that the dispersion in grain volumes be measured without ambiguity and be accurately representable by using a single parameter. The experimental observation that the grain volume distributions are consistently well approximated by the lognormal function agrees well with other naturally occuring systems, and offers a convinient mathematical description of the global microstructure. Note that this statement in no way implies that the lognormality is purely coincidental: as shown later, the genesis of the distribution function has a direct connection to the manner in which recrystallization nuclei are dispersed in the polycrystal volume.

---

[2] Private communication.

2.2 Experimental Methods

2.2.1 Material

High purity aluminum was chosen as the material for this research for the following reasons:

(1) Aluminum containing low impurity levels exhibits a single phase microstructure with few annealing or deformation twins.

(2) It is easily separated into its component grains through grain boundary penetration with liquid gallium.

The material was received from two sources. That labeled as “super purity” (S.P.) was received from Consolidated Aluminum Co., Jackson, Tenn. [72Con], and that labeled as “high purity” (H.P.) from the ALCOA Technical Center, Pittsburgh, PA. The S.P. material was consumed during the initial series of experiments, and hence, for the

Table 2.2
Chemical Composition of Aluminum Used in the Study
Composition in Weight (%)

	Designation	
Element	S.P.	H.P.
Al	99.9980	99.985
Si	0.0003	0.001
Fe	0.0009	0.001
Cu	0.0001	0.004
Mg	0.0005	0.002
Ca	0.0002	0.003
B	---	0.003
Na	---	0.001

subsequent experiments, H.P. material was used. The composition of both the grades is given in Table 2.2 below.

2.2.2 Thermomechanical Treatments

The material was given a series of thermo-mechanical treatments with the aim of arriving at a series of samples containing (nominally) the same grain boundary area per unit volume, but different grain volume distribution widths. Because of a higher impurity content and coarser initial cast structure, the H.P. samples were prepared by using an additional deformation step and a higher annealing temperature. The sequence of treatments used is given below.

Blocks of sound material were sawed from the commercially supplied ingots. Block dimensions for the S.P. samples were, 6.35 cm x 6.35 cm x 10.16 cm (2.5" x 2.5" x 4"), and for the H.P. samples, 7.62 cm x 7.62 cm x 10.16 cm (3" x 3" x 4").

During the subsequent forging and rolling treatments, the blocks were cooled in liquid nitrogen (77K) before and intermittently during the treatment. This prevented dynamic recrystallization and also made it possible to obtain a more homogeneous deformation [57Car]. Between each thermo-mechanical treatment, the blocks were sawed to a regular shape (so as to remove any odd angles and folds), and cleaned in 10 v/o HF.

The recrystallization temperatures and times for both series were determined by examining the microstructure on two mutually perpendicular planes so as to insure that the samples were fully recrystallized with an equiaxed and homogeneous grain structure.

The blocks were drop-hammer forged to successive 50% reduction in thickness in three mutually perpendicular directions in order to achieve a uniform grain structure and then given a recrystallization anneal. In the case of S.P., the recrystallization was carried out in a recirculating air furnace at a temperature of 450 ± 1°C for 10 minutes, and for H.P., in a neutral salt bath furnace at a temperature of 510 ± 2°C for 10 minutes.

The H.P. samples were given a further 45% reduction in thickness by rolling and then recrystallized as before. In the case of S.P., this step was omitted since after the forging-recrystallization treatment, the structure was found to be equiaxed and homogeneous.

For both S.P. and H.P., these recrystallized samples constituted the starting material used to produce a series of samples with varying grain volume distribution widths. The grain volume distribution widths were established by imparting a prescribed amount of cold work to the samples (defined as the % reduction in thickness by rolling). The sample designation is based on this step and is as given below in Table 2.3.

The findings of Richards and Pugh [59Ric] indicate that pure aluminum does not develop a pronounced deformation texture up to 60% reduction in rolling. Hence, the upper limit of deformation was set at 60%. Also, two blocks of material (designated as H.P.(1) and H.P.(1a)) were given identical thermomechanical treatments to test the reproducibility of the correlation between the deformation history and the grain volume distribution width.

After rolling reductions, the samples were cooled with liquid nitrogen and sawed 2.54 cm (1 inch) from each end along the length and 1.27 cm (0.5 inch) from each side along the width in order to remove the material which had deformed in excess of the

Table 2.3
Final deformation by cold rolling prior to recrystallization and the corresponding sample designation.

Series	Designation	% Cold Work	True Strain
S.P.	SP(1)	50	0.405
	SP(2)	45	0.372
	SP(3)	40	0.336
	SP(4)	10	0.095
	SP(5)	5	0.049
	SP(6)	2	0.02
H.P.	HP(1)	60	0.47
	HP(2)	40	0.336
	HP(3)	30	0.26
	HP(4)	25	0.22
	HP(5)	20	0.18
	HP(6)	15	0.14
	HP(7)	10	0.095
	HP(8)	7.5	0.07

prescribed amount. This step was not necessary for deformations lower than 15%. The blocks were cleaned, given a recrystallization anneal, and used to obtain three types of information:

(a) The change in grain boundary and per unit volume (S_V) as a function of annealing time during isothermal annealing,

(b) the grain volume distribution, and

(c) the tensile properties.

2.3 Determination of the Grain Volume Distribution

The method employed in the present study for determining the grain volume distribution is based on embrittling polycrystalline aluminum by liquid gallium penetration of the grain boundaries. The penetration phenomenon is driven by a reduction of the total surface energy through wetting of grain boundaries by the liquid metal. The technique of separating individual grains from an aggregate was first used by Desch [19Des] in 1919. Employing mercury, he separated grains from a β-brass casting.

2.3.1 Embrittlement Characteristics

Examination of the Al-Ga system [83Mur], Figure 2.1, shows that it conforms to the general requirements for susceptibility to grain boundary penetration [60Ros]. These are: (1) low intersolubility, (2) an absence of intermetallic compounds, and (3) the occurrence of a low melting eutectic adjacent to the lower melting component. These conditions are

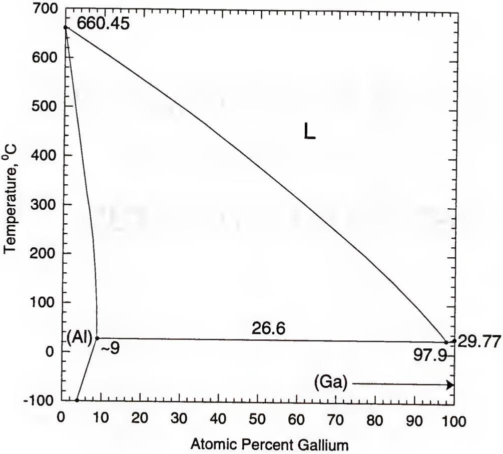

Figure 2.1 The Al-Ga equilibrium phase diagram [83Mur].

necessary but not sufficient for complete penetration. In addition, as suggested by Smith [48Smi], the relative surface energies must be considered. Aluminum, being slightly soluble in gallium, starts to dissolve, leading to the formation of a liquid of composition dictated by the separation temperature and the Al-Ga system equilibria.[3] If the dihedral angle between aluminum and the liquid is zero, the dissolution process continues and grain boundary penetration takes place. Although no attempt was made to measure the dihedral angle, it can be assumed to be close to zero because of the extremely rapid penetration rates.[4] Penetration along grain boundaries is illustrated in Figure 2.2. The scanning electron micrograph was in the back scattered electron mode shows atomic number contrast. The higher atomic number gallium-rich liquid is seen to be distributed along the grain boundaries as a thin white layer.

2.3.2 Embrittlement and Separation Procedure

Based on the grain boundary area per unit volume (S_V) in the sample, the amount of gallium required for penetration was estimated beforehand. Metallographic measurements indicated that under the penetration conditions specified below, the average penetration thickness at the grain boundaries was approximately 5×10^{-4} cm. Thus for example, for a sample with a total grain boundary area of 100 cm^2, the gallium requirement was 0.05 cm^3 or 0.3 gm. It was found that the actual amount of gallium required was approximately 20% in excess of that calculated to allow for coating of the external surfaces. The sample size

---

[3] Upon cooling to room temperature, the composition of the liquid was (as expected) close to that of the eutectic.

[4] It was found that at 50°C, the penetration depth was > 2 cm in less than 30 minutes.

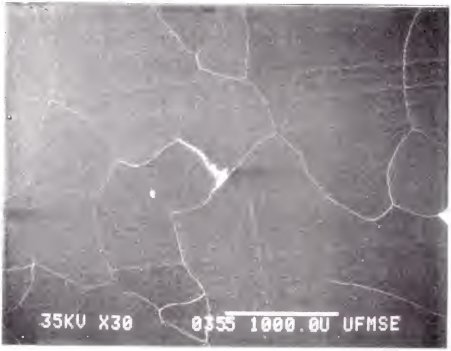

Figure 2.2 Back scattered electron micrograph illustrating gallium distribution along aluminum grain boundaries. Embrittlement conditions: 50°C for 10 minutes.

was based upon the grain size, however, even for a coarse grained sample (e.g., $S_v = 4$ mm^2/mm^3), a 1.25 cm cube was sufficient for valid statistical estimates.

In order to thin the existing oxide layer on the outer surface, the sample surface was ground to a 400 grit SiC finish, followed by a two minute immersion in 10 v/o HF. The sample was put on a clean, dry glass slide and heated to 50°C on a hot plate. The required amount of gallium was placed on the sample and the surface beneath the drop was scratched with a sharp knife. This allowed the gallium to come in contact with aluminum beneath the thinned oxide layer and assured the start of penetration. The sample was covered with a dry glass beaker and penetration was allowed to proceed for ten to fifteen minutes. The penetration was deemed to be complete when some gallium had collected at the bottom surface, leaving only a thin film at the top. It was interesting to note that when the sample was upended, the liquid gallium collected at the bottom went through the sample like a sieve.

If the upper surface had only a thin film of gallium left with none collected at the bottom, a small amount (< 0.1 gm) of gallium was added, resulting in a complete penetration in two to three minutes. As discussed later, the penetration time was kept to a minimum.

After complete penetration, the external surfaces were coated with excess gallium, and the sample was cooled to room temperature. The cooled sample was placed in a hand vice and squeezed gently until small cracks appeared on the surface. These cracks were opened with a sharp knife to disintegrate the sample into several big pieces.

External surfaces containing partial grains were removed and discarded in order to eliminate them from the statistics. The central portions yielded several clumps of grains.

Approximately 500 to 2000 grains give a good statistical distribution without making the analysis unnecessarily laborious. For this reason, two or three clumps were selected for further separation and analysis. The remaining clumps were stored in glass tubes for future use. The clumps were further separated into individual grains with tweezers and a dissecting needle under a low power stereomicroscope.

In the case of clumps which resisted further separation, the distinction between an incompletely penetrated group of grains and a coarse single grain could be easily made on the basis of the presence (or absence) of reentrant angles between facets. The incompletely penetrated groups were retreated with a drop of gallium and then separated as before.

A fractograph of an embrittled sample, Figure 2.3, shows grains of different sizes and shapes distributed in space. Several reentrant angles are indicated by arrows. Complete separation at the grain boundaries is illustrated in Figure 2.4. The fracture leaves sharp facets without any evidence of plastic deformation.

The separated grains were put in a glass beaker with 50 ml of distilled water. A vigorous exothermic reaction, due to the formation of a surface oxide, emulsified the gallium. The supernant liquid was carefully decanted and the procedure repeated until clear water remained. The reaction products remaining on the grain surfaces were removed by ultrasonic cleaning in acetone followed by drying on a hot plate.

The cleaned and dried grains were examined under the stereomicroscope to insure that the separation was complete. Occasionally, two or three grains remained stuck

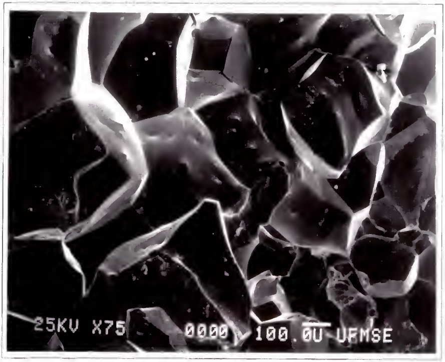

Figure 2.3 Secondary electron fractograph of Ga-embrittled aluminum sample surface. Embrittling conditions: 50°C for 10 minutes. Reentrant angles between grain surfaces are shown by arrows.

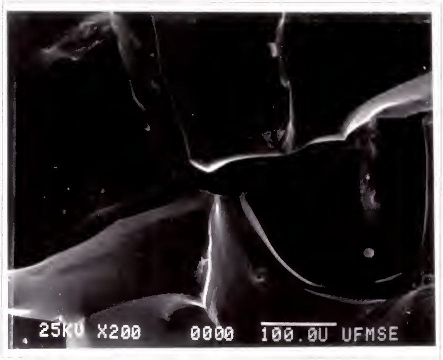

Figure 2.4 Secondary electron fractograph of Ga-embrittled aluminum sample surface. Embrittling conditions: 50°C for 10 minutes. Higher magnification than Figure 2.3 shows separation at grain surfaces. Lack of surface deformation indicates classical grain boundary embrittlement.

together. These were separated by cutting along the grain boundaries. The grains were then sieved to give a rough classification. Each sieve class was subdivided into two or more subclasses according to size. The grains in each subclass were counted under the stereomicroscope and stored in glass tubes for weighing. All the weighing was done on a Mettler electronic balance with at least count of .001 mg. The coarser grains were weighed individually, while the finer grains were weighed as a group. The grouping of finer classes did not introduce an error since the size distributions generated would employ grouped data. A sample of separated grains is shown in Figure 2.5.

2.3.3 Separation Efficiency and Metal Loss

Reproducibility of the data depended upon two factors: efficiency of the grain separation process and metal loss through gallium-aluminum interaction. It was difficult and laborious to ensure a high separation efficiency when the sample size was large. As suggested earlier, a sample of about 500 to 2000 grains could be separated completely without affecting the accuracy of subsequent statistical analysis.

Although loss of aluminum through interaction with gallium is an inherent aspect of this method, the loss can be minimized by optimizing the penetration time and temperature. Metallographic examination of a series of samples embrittled for varying lengths of time and at temperatures ranging from 40 to 150°C indicated that 15 minutes at 50°C was optimum for a 1.25 cm thick sample of coarse-grained (S_v of 3 to 10 mm^2/mm^3) pure aluminum. The distribution of gallium under these conditions is illustrated in Figure 2.6. This time-temperature combination gave a metal loss of approximately 5.7 w/o. Assuming

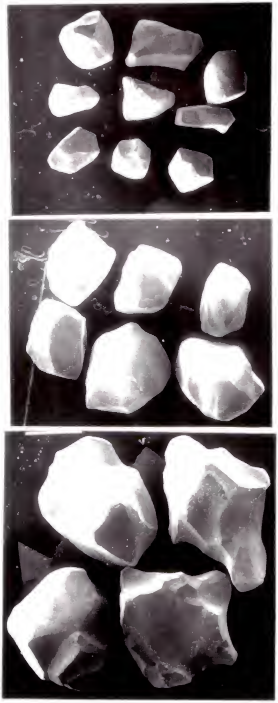

Figure 2.5 Separated aluminum grains.

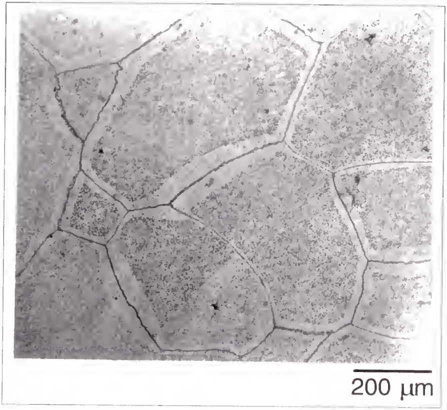

Figure 2.6 Optical micrograph illustrating volume diffusion of gallium in aluminum. Embrittlement conditions: 150°C, 15 minutes, resulting in a high aluminum loss.

the average grain to be regular TKD, this converted to a loss in thickness of 3.96 x 10^{-4} cm. Thus, grains smaller than about 8 μm were lost in the separation process.

At temperatures lower than 50°C, the penetration time was significantly longer (> 60 minutes) and resulted in an uneven penetration, while a significantly higher metal loss was incurred if the penetration was carried out at a higher temperature and/or a longer time. For example, a penetration carried out at 150°C for 15 minutes gave a metal loss of 16 w/o. Higher temperatures and/or longer times lead to an increase in the boundary layer thickness, resulting in a higher metal loss. The resultant boundary layers are illustrated in Figure 2.6.

Grain surfaces in one sample were examined by using an ORTEC energy dispersive x-ray unit to determine the surface composition. In all cases examined, gallium was present in very small amounts. Figure 2.7(a) shows the ED spectrum of a separated and cleaned crystal in auto range, while Figure 2.7(b) shows the same spectrum on an expanded scale. It can be seen from 2.7(b) that only traces of gallium are present on the surface. It was thus concluded that residual surface gallium would not introduce any significant error into the calculation of the grain volume distribution.

2.4 Results

All of the samples studied in this investigation yielded distributions which were unimodal and (positively) skewed towards the smaller grain sizes. A frequency histogram of sample H.P.(1) is plotted in Figure 2.8(a) to illustrate the typical form of the distributions.

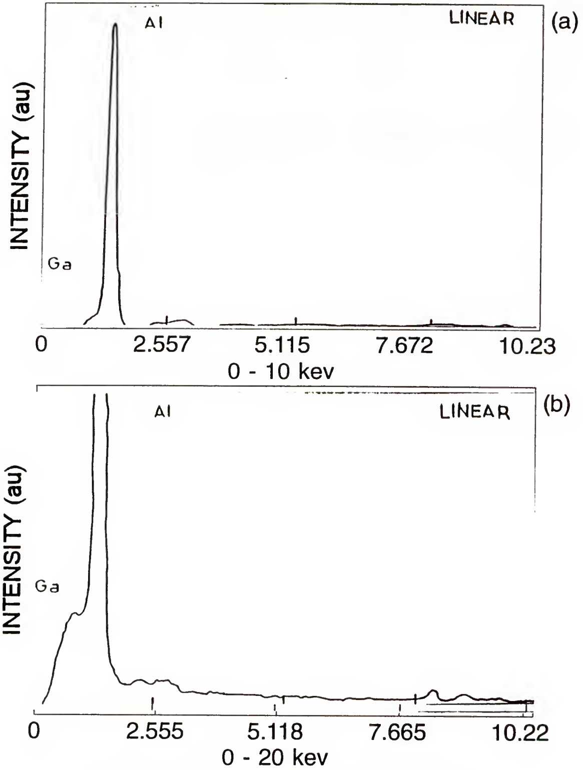

Figure 2.7 (a) EDS from the surface of a separated and cleaned aluminum grain. (B) Same spectrum shown on an expanded intensity scale, showing trace amounts of Ga.

It has been known since 1879 that a transformation of the variate (weight in the present investigation) to its logarithm may successfully transform a skewed distribution such as the one shown in Figure 2.8(a), into one which is more or less symmetrical. Figure 2.8(b) shows a comparison between the shape of the distribution before and after the transformation, again using the data of sample H.P.(1). It can be seen that through the transformation to ln(weight), an approximately symmetrical form is obtained. In cases where the logarithmic transformation successfully removes the skewness, the distribution can be approximated as being log-normal. As mentioned earlier, several previous studies have shown that distributions in a wide variety of systems can be well approximated as being log-normal.

The log-normal function is obtained by substituting the logarithm of the variable into the normal probability density function [73Ait] and is given by:

$$y = \frac{1}{\sqrt{2\pi}\,\ln\sigma_g}\frac{1}{x}\exp\left[-\frac{1}{2}\left(\frac{\ln x - \ln\mu_g}{\ln\sigma_g}\right)^2\right] \qquad (2.1)$$

where, $\ln\mu_g$ is the arithmetic mean of $\ln x$; i.e., μ_g is the geometric mean of x. $\ln\sigma_g$ is the arithmetic standard deviation of $\ln x$, i.e., σ_g is the geometric standard deviation of x. $\ln\mu_g$ and $\ln\sigma_g$ are given by equations 2.2 and 2.3, respectively,

$$\ln\mu_g = \frac{1}{N}\sum_{i=1}^{N}\ln x_i \qquad (2.2)$$

$$\ln\sigma_g = \left[\frac{\sum_{i=1}^{N}(\ln x_i - \ln\mu_g)^2}{N-1}\right]^{\frac{1}{2}} \qquad (2.3)$$

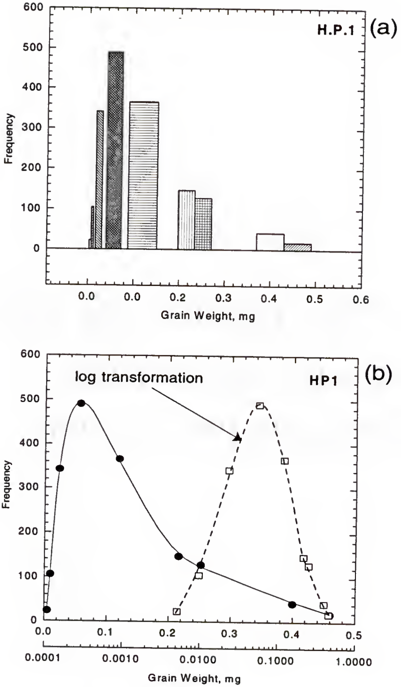

Figure 2.8 (a) A frequency histogram illustrating the lognormal distribution in sample HP1. (b) Shows the removal of positive skew via a logarithmic transformation of the variable (grain weight).

The most straightforward way to test an experimentally determined distribution is to plot the cumulative frequency on a probability scale versus the log of the variable. The log-normal distribution gives a straight line on such plots [48Dal], as shown in Figure 2.9, again using the data of HP(1). Analogously, the normal or gaussian distribution gives a straight line when the variable itself (instead of its logarithm) is used.

Using this representation, the geometric mean and standard deviation of the distribution can be estimated. By convention [33Dav], the geometric mean is given by the value of Ln(weight) at 50% cumulative frequency,

$$\ln \mu_g = \ln X\big|_{50\% C.F.} \tag{2.4a}$$

The geometric standard deviation is inversely proportional to the slope of the line and is given by,

$$\ln \sigma_g = \frac{\ln X\big|_{84\% C.F.} - \ln X\big|_{16\% C.F.}}{2} \tag{2.4b}$$

The accuracy of the values obtained, however, depends upon the accuracy with which the straight line is drawn through the data points. For this reason, the values of the mean and the standard deviation reported were calculated by using equations 2.2 and 2.3, respectively. Such straight line plots, however, have a dual use. First, as mentioned earlier, they allow a quick check on the assumption of the log-normality, and second, they can be used to estimate the linear regression correlation coefficient, thereby providing a formal check on the validity of fitting a straight line to the data.

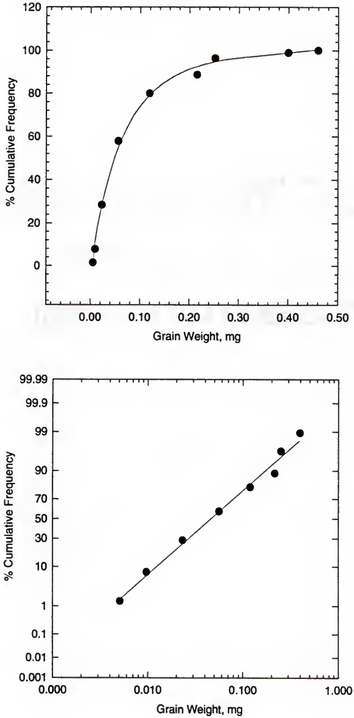

Figure 2.9 Cumulative frequency plots for HP(1). (a) Linear scales, (b) log-probability scales.

2.4.1 Tests of Lognormality

Several tests are available for checking the validity of the assumption of log-normality. Of these, the three most important, i.e., kurtosis, skewness and the X^2 goodness-of-fit tests [33Dav] were employed. The X^2 goodness-of-fit test however had to be abandoned for reasons mentioned below.

For calculation of the X^2 value, the theoretical frequency in each size class was computed by calculating the area occupied by a class interval. A numerical integration procedure of the distribution function within the limits of each class was used for the purpose. It was found that, for each distribution, the observed frequency of one or two size classes differed significantly from the theoretically expected value. This increased the X^2 value to a level where the assumption of log-normality was forced to be rejected. The frequency of all the other size classes, however, varied very little from their theoretically expected value. Further analysis revealed the cause of rejection:[5] for the purposes of carrying out the X^2 test, the original grouped data had to be converted into intervals. However, the test is extremely sensitive to the width of the intervals, and within limits, the value of the X^2 could be changed by merely adjusting the intervals. For this reason, the test was abandoned. All the other goddess-of-fit tests also require ungrouped data; thus kurtosis, skewness, and the linear regression correlation coefficient (of the log-probability plots) were employed instead.

---

[5] Private communication with R.L. Scheffer.

2.4.2 Data Analysis

The lognormal function possesses moments of any order. The *j*th moment about the origin is given by:

$$\lambda_j = \exp(j \ln \mu_g + \tfrac{1}{2} j^2 \ln^2 \sigma_g) \tag{2.5}$$

Using the properties of the moment generating function of the normal distribution, the arithmetic mean and standard deviation are given by:

$$\mu_A = \exp(\ln \mu_g + \tfrac{1}{2} \ln^2 \sigma_g) \tag{2.6}$$

$$\begin{aligned} \sigma_A^2 &= \exp(2 \ln \mu_g + \ln^2 \sigma_g)[\exp(\ln^2 \sigma_g) - 1] \\ &= \mu_A^2 \eta^2 \\ &\text{where} \\ \eta^2 &= \exp(\ln^2 \sigma_g) - 1 \end{aligned}$$

From the definition, it can be seen that the coefficient of variation (the ratio of the arithmetic standard deviation and the mean) is given by η. It is thus clear that distributions with identical standard deviations have the same coefficient of variation.

The measures of departures from normality, i.e. the coefficient of skewness (γ_1) and the coefficient of kurtosis (γ_2) are given by [73Ait]:

$$\gamma_1 = \frac{\lambda_3}{\mu_A^3} \tag{2.7a}$$

$$\gamma_2 = \frac{\lambda_4}{\mu_A^4} - 3 \tag{2.7b}$$

Based on the results of the calculation of the above parameters, it was clear that all the grain volume distribution data in this investigation were consistently well approximated by the lognormal function. Figure 2.10 illustrates two extremes of the grain volume

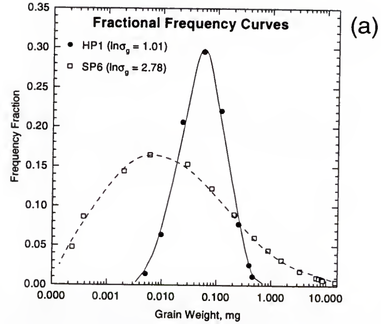

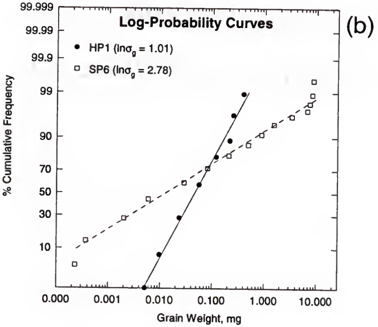

Figure 2.10 Frequency curves for two extremes of the grain volume distribution widths in the present investigation. (a) Fractional frequency vs grain weight on a logarithmic scale. (b) Linear representation of the %cumulative frequency-grain weight data on log-probability scales.

distributions obtained in the present investigation. It can be seen that the distribution with the higher width shows a significantly greater skew compared to the one with the smaller distribution width.

2.4.3 Effect of Strain Prior to Recrystallization

This section deals with the question of how the microstructure is modified as a results of the degree of deformation imposed prior to recrystallization and annealing. The modification is defined through the use of $\ln\sigma_g$ since it is most sensitive to the range of grain sizes obtained.

Table 2.4 reports the percent cold work prior to recrystallization and annealing and the resulting distribution widths for both S.P. and H.P. samples. The sample treatments are as given earlier in the section on procedure. As noted earlier, the sample designated by H.P.(1a) was prepared in exactly the same manner as H.P.(1) to test the reproducibility of the relation between the cold work and the distribution width. It can be seen from Table 2.4 that the reproducibility is indeed very good. Since there was no significant difference between these two samples, henceforth they will be referred to by the single designation H.P.(1).

The data presented in Table 2.4 are plotted in Figure 2.11(a), along with the results of least squares curve fitting discussed below. The data of Patterson [78Pat] on high purity aluminum are included for comparison. It can be seen that for both S.P. and H.P. samples, the distribution width decreases monotonically with increasing amounts of cold work, the

Table 2.4

Summary of Sample designation and corresponding values of the % deformation imparted in the final cold rolling stage, along with the grain volume distribution widths after recrystallization.

Sample	%Cold Work	True Strain	$\ln\sigma_g$
SP(1)	50	0.405	1.21
SP(2)	45	0.372	1.28
SP(3)	40	0.336	1.35
SP(4)	10	0.095	1.78
SP(5)	5	0.049	2.23
SP(6)	2	0.02	2.79
HP(1)	60	0.47	1.01
HP(1a)	60	0.47	1.01_2
HP(2)	40	0.336	1.13
HP(3)	30	0.26	1.15
HP(4)	25	0.22	1.17
HP(5)	20	0.18	1.22
HP(6)	15	0.14	1.25
HP(7)	10	0.095	1.31
HP(8)	7.5	0.07	1.33

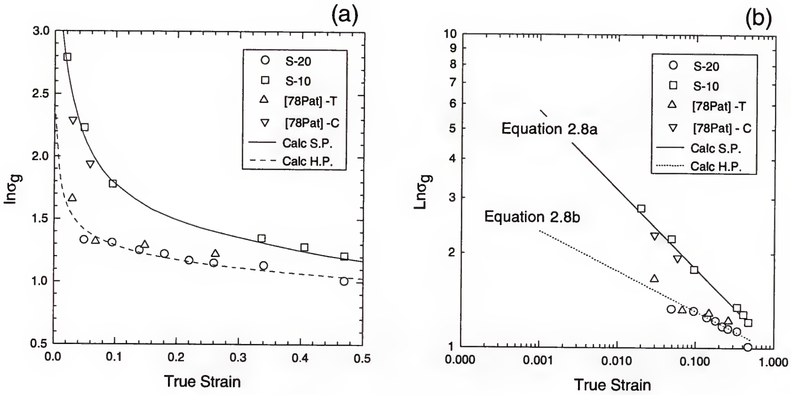

Figure 2.11 The dependence of grain volume distribution width on the thermomechanical history of samples. The grain volume distribution width is plotted as a function of the final deformation step. (A) Raw data. (B) Data plotted on logarithmic axes illustrating the power-law dependence. Also shown are linear fits based on equation 2.8(a) and 2.8(b) for S.P. and H.P. series, respectively.

dependence being quite strong at low deformation levels. This agrees well with Patterson's [78Pat] findings on pure aluminum. Each series is, however, quite distinct.

It may be recalled that the deformation histories of S.P. and H.P. samples was different in that the H.P. samples were given an additional 45% reduction by cold rolling (i.e. over and above that for the S.P. samples) at the pre-final stage. It can be seen from Figure 2.11(a) that at comparable final deformation levels, the S.P. samples exhibit higher distribution widths than the H.P. samples. Patterson's [78Pat] data also reinforces this finding. In his case, the 'C' series samples were given an additional 50% reduction in forging over that for the 'T' series. Patterson however plotted the data for both the 'C' and 'T' series on a single curve, most probably because of the limited amount of data available at the time.

Based on Figure 2.11(a), it is clear that the grain volume distribution width is a function of the mechanical history of the sample, and may perhaps be traceable even to the distribution established during solidification. The modification of the structure through an increase or decrease of the distribution width at each successive stage is seen to depend upon the severity of the deformation imposed.

In order to explore the effect further, curve fitting was used for each series of samples. In both cases, a power law relationship gave the best fit. Thus,

$$\ln\sigma_g = 0.99\varepsilon_t^{-0.253} \tag{2.8a}$$

$$\ln\sigma_g = 0.97\varepsilon_t^{-0.128} \tag{2.8b}$$

The regression correlation coefficients for equations 2.8a and 2.8b (S.P. and H.P. respectively), were 0.980 and 0.975, indicating a good fit to the data in each case. The equations, along with the experimental data, are plotted on a log-log scale in Figure 2.11(b) in order to illustrate the power-law behavior. Using the parameters of these equations (which are strictly valid only within the experimental range), a further insight can be gained in the process of microstructural modification in terms of the evolution of the grain volume distribution width. Thus, for example, it is possible to calculate the final deformations necessary to obtain the grain volume distributions widths of H.P. series on the basis of the equation applicable to the S.P. series and vice versa using the parameters of equations 2.10(a) and 2.10(b). Tables 2.5(a) and 2.5(b) list the results of this calculation for the S.P. and H.P. series, respectively. Table 2.5(a) lists the experimental values for H.P., while column 3 lists the amount of final deformation that would be required to achieve a particular distribution width if the samples were in the condition of S.P. In the Table 2.5(b), the positions of S.P. and H.P. are interchanged.

It is clear from the results that decreasing the amount of pre-final deformation leads to an increase in the amount of final deformation needed to achieve a particular distribution width. Interestingly enough, the reverse also seems to be true, i.e., increasing the amount of deformation at the pre-final step decreases that required at the final step. The process is not, however, one of the simple addition, indicating that the intervention of a recrystallization and annealing step somehow modifies the effect of each successive deformation.

Another possible result of such modification is the possibility that at each step in the process, there appear to be upper and lower limits to the distribution widths which can be achieved by a single deformation step. For example, consider the first row in Table 2.5(a). In order to achieve a standard deviation of 1.01, calculation on the basis of equation 2.8(a) gives a value of 152% for the deformation required. This clearly suggests a requirement for

Table 2.5(a)

The grain volume distribution widths and % final stage cold deformation by rolling for H.P. series. Column 3 lists the final deformation level necessary to obtain the same grain volume distribution width if the samples were in a microstructural state of the S.P. series (equation 2.8a).

$\ln\sigma_g$	% Cold Work	% Cold Work Extrapolated From Equation 2.8(a)
1.01	60	152
1.13	40	81
1.15	30	74
1.17	25	68
1.22	20	55
1.25	15	54
1.31	10	39
1.33	7.5	37

Table 2.5(b)

The grain volume distribution widths and % final stage cold deformation by rolling for S.P. series. Column 3 lists the final deformation level necessary to obtain the same grain volume distribution width if the samples were in a microstructural state of the H.P. series (equation 2.8b).

$\ln\sigma_g$	% Cold Work	% Cold Work Extrapolated From Equation 2.8(b)
1.21	50	20
1.28	45	12
1.35	40	8
1.78	10	0.9
2.23	5	0.2
2.79	2	0.03

an intermediate recrystallization step. Thus, even though equations 2.8(a) and 2.8(b) are not derived from theoretical considerations, a useful insight into the direction of modification of the grain volume distribution is gained through their use.

So far, the discussion has centered only around the effect of deformation at the final and pre-final stage. It is likely that other factors such as the development of a crystallographic texture, annealing temperature, deformation temperature, and the state of imposed stress (i.e., tensile, compressive, torsional, etc.) may also have an effect of the resulting distribution width. An experimental treatment of this aspect is however outside the scope of this investigation and must await a more detailed study.

2.4.4 Transformation of the Variable

It is sometimes desirable to know the properties of distributions which arise through some transformation of the variable. Specifically, in the case of grain volume distributions, the form and parameters values of grain diameter[6] or surface area distributions may be of interest. In such cases, assuming a constant shape factor, it can be shown that if the volumes are distributed log-normally, the distributions derived therefrom are also log-normal, and that the distribution parameters of the tow are simply related. Formally, if the variable $X = kD^m$ is log-normally distribution, then so is D (and the converse is also true.). Furthermore,

---

[6] It is of course well known that grains do not possess either a unique "diameter", or a constant shape factor which is independent of size. However, a degree of simplification in subsequent analysis is obtained through these assumptions, and may sometimes override such considerations.

$$\ln \mu_{g(D)} = \frac{1}{m} \ln\left(\frac{\mu_{g(X)}}{k}\right) \tag{2.9a}$$

and

$$\ln \sigma_{g(D)} = \frac{1}{m} \ln \sigma_{g(X)} \tag{2.9b}$$

Having seen that the distribution of grain volumes is log-normal, it is fruitful to consider the origins of the process through which the distribution may evolve. By doing so, we may then gain a useful insight into the underlying natural causes. The next section gives a brief description of the evolution of the log-normal distribution, and points out the special restrictions placed on the process in its application to recrystallization and grain growth.

2.5 Genesis of the Lognormal Distribution

In 1903, Kapteyn [03Kap] first proposed a formal framework which leads to a log-normal distribution of the variable as follows: suppose that the value of a variable X is initially X_0 and after the *j*th step in the process, it is X_j, reaching a final value of X_n after n steps. If it is assumed that at the *j*th step, the change in the variable is a random proportion of a function $\phi(X_{j-1})$ of the value X_{j-1} already attained, then,

$$X_j - X_{j-1} = \varepsilon_j \phi(X_{j-1}) \tag{2.10}$$

where the set $\{\varepsilon_j\}$ is mutually independent and also independent of the set $\{X_j\}$. For the special case where the function $\phi(X) = X$, i.e. the change in the variable is a random proportion of the momentary value of the variable, the law of proportionate effect is said to be in operation.[7] For this case, equation 2.10 reduces to

$$X_j - X_{j-1} = \varepsilon_j X_{j-1} \tag{2.11}$$

Equation 2.11 may be rewritten as

$$\frac{X_j - X_{j-1}}{X_{j-1}} = \varepsilon_j, \text{ and}$$

$$\sum_{j=1}^{n} \frac{X_j - X_{j-1}}{X_{j-1}} = \sum_{j=1}^{n} \varepsilon_j$$

If we assume that the effect at each step is small, so that

$$\sum_{j=1}^{n} \frac{X_j - X_{j-1}}{X_{j-1}} \cong \int_{X_0}^{X_n} \frac{dX}{X} = \ln X_n - \ln X_0,$$

$$\text{giving} \tag{2.12}$$

$$\ln X_n = \ln X_0 + \varepsilon_1 + \varepsilon_2 + \ldots + \varepsilon_n$$

By the classical additive form of the central limit theorem [22Lin, 25Lev], it can be seen that $\ln X_n$ is asymptotically normally distributed and hence X_n is asymptotically lognormally distributed.

2.5.1 Evolution During Recrystallization

Certain restrictions are placed in applying the above treatment to the process of recrystallization. The process may be thought of as occurring through one of several mechanisms including strain induced boundary migration [50Bec,60Bai,74Mor] and subgrain growth [63Wei,74Mor,78Kre]. The sites at which recrystallization starts are generally sites of high stress concentration [45And], the size of the emerging recrystallized grains being then controlled by the local growth rate and the distance from its neighbors. Thus, the placement of these sites becomes as important consideration. It has been observed that the placement and density of these sites is dependent upon the degree of deformation, being clustered and relatively low at low levels of deformation and random and more dense with increasing deformation levels [63Wei].

---

[7] The law of proportionate effect may be stated formally by paraphrasing Aitchison and Brown [73Ait] as: a variable subject to change is said to obey the law of proportionate effect if the change in the variable at any step of the process is a random proportion of its previous value.

Patterson [78Pat] hypothesized that at places where the clustering is present, an early impingement would restrict the growth while allowing others to grow to larger sizes. Even in this context, however, one may expect the law of proportionate effect to be operative, leading to a log-normal distribution of grain sizes, the width of the distribution being controlled by the density and placement of the nucleation sites. Thus, the degree of prior deformation controls the distribution width while the law of proportionate effect controls its form.

The studies of Weismann et al. [63Wei] on dislocation arrangements during recrystallization of high purity aluminum have shown that up to about 5% cold work, mainly dislocation tangles are present, changing to cells with well delineated dislocation boundaries at about 30% cold work. With a further increase in cold work, the dislocation density at the cell walls increases, while the cell size remains essentially constant. This indicates that there is a rapid initial increase in the number of possible nucleation sites up to about thirty percent cold work, at which point the density stabilizes, increasing only slowly with additional deformation. This agrees well with the experimentally observed dependence of the grain volume distribution width on cold deformation prior to final recrystallization (a power law relationship with a negative exponent, Figure 2.11(a) and equations 2.8(a),(b)).

2.5.2 Cell Area Calculations

In the present investigation, the form of cell area distributions was by generating two dimensional cells as follows: pairs of random number were generated to define the coordinates of the centers of the cells. Each cell center was then assigned a "growth potential" or initial dimension, again through a set of random numbers. The growth rate of each cell was then assumed to be proportional to its immediate size (the law of proportionate effect). Thus,

$$\text{Growth Rate} = \frac{dR}{dt} \propto R$$
$$= kR, \text{ Therefore,}$$
$$\frac{dR}{R} = kdt$$

Integrating within the limits of initial and “impingement” radii,

$$\int_{R_0}^{R_{im}} \frac{dR}{R} = k\int_0^t dt \text{ and}$$
$$\ln\left(\frac{R_{im}}{R_0}\right) = kt$$

The governing growth equation is,

$$R_{im} = R_0 e^{kt} \tag{2.13}$$

where k is a constant of proportionality and R_{im} is the value of the cell radius at impingement with neighbor. For each cell center, the growth equation was solved pairwise with its neighbors, thus defining the boundaries of the cell.

These calculations yield a distribution of cell areas which is approximately log-normal. The results of one such computation are shown in Figure 2.12(a) to (c). Figure 2.12(a) shows the resulting cells (24 nucleation sites), while a histogram of the cell areas and cumulative frequency plot on log-probability scales (60 cell areas) is shown in figures 2.12(b) and (c), respectively. It can be seen that the cell areas are approximately lognormally distributed with a characteristic positive skew. Kottler [50Kot] also used a similar treatment for particle size distributions, again arriving at a log-normal distribution of particle sizes if their nucleation times were normally distributed. It may be noted that the above treatment is somewhat artificial since the resultant cells do not correspond to an equilibrium cell structure.

2.5.3 Constancy of the Grain Volume Distribution Width

Application of the law of proportionate effect to grain growth leads immediately to an apparent contradiction. The law suggests that the longer the process is in operation, the more should be the inequality between grain volumes, leading to a continuous increase in the distribution width with time of anneal. This is in conflict with the observation that the distribution width remains essentially unchanged during steady-state grain growth in aluminum [82Rhi2] and titanium [72Oka]. Kalecki [45Kal], having encountered a similar anomaly in the distribution of incomes, suggested a method by which special stabilizing influences could be taken into account, which then forced the distribution width to remain constant during the process, while the distribution itself remained log-normal.

In the case of steady state grain growth, the origin and nature of width-stabilizing sources is not clear at the present time. It is possible that the topological events which must

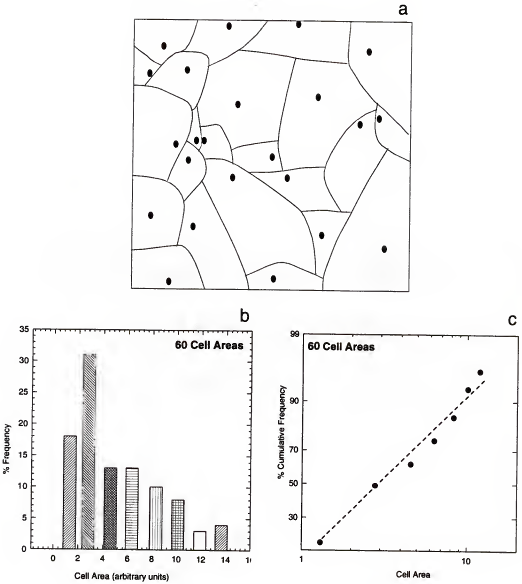

Figure 2.12 Generation of cell areas using a random placement of nuclei and the law of proportionate effect. (A) A representative section of approximately 20. (B) Frequency histogram of 60 cell areas cells showing a positive skew in the distribution. (C) Same data plotted on log-probability scales, with a linear fit indicating a lognormal distribution.

be traversed play a role [74Rhi, 82Rhi2]. In particular, the frequency of 3-sided faces is tied to the grain volume distribution width (increasing monotonically with increasing width) and is also required by the topological model to remain constant during grain growth. It thus appears likely that once a steady state grain growth is established, the frequency of 3-sided faces will remain constant due to topological constraints and so will the grain volume distribution width. It must be stressed, however, that the connection between the grain volume distribution width and the frequency of 3-sided faces has been observed experimentally and not established from theoretical considerations.

CHAPTER 3

MECHANICAL BEHAVIOR OF ALUMINUM POLYCRYSTALS

3.1 Introduction

This chapter reports the direct experimental identification of a new and relatively subtle microstructural parameter which significantly affects all aspects of plastic deformation of polycrystals. The polycrystals used for the study were obtained from two purities of aluminum, both of which can be termed as "high purity" in engineering terms, i.e. with the total metallic impurities not exceeding 0.01 at.%, and tested in uniaxial tension at a constant temperature of 77 K and the same initial strain rate. The microstructural parameter was identified as the width of the grain size distribution, using grain weight (or volume) as an unambiguous measure of size. The use of such a parameter allows a succinct and global description of the polycrystal microstructure and can reveal aspects of polycrystal response which may otherwise be masked if a simple averaging procedure is used instead.

Many studies of the grain size-flow stress relationship obtain the various levels of grain sizes by varying the extent of pre-recrystallization deformation. As shown in the last chapter, this not only changes the "average grain size," but also the width of the grain size distribution. It follows that one now has to take into account not only one but at least two parameters in the interpretation of property values. In such instances, attributing the microstructural response (e.g. change in flow stress per unit strain) solely to changes in the average grain size is valid only if the grain volume distribution exerts no influence.

As shown in the results section of this chapter, when the effect of grain size distribution is separated from the effect of average grain size (as determined from random two-dimensional sections through the microstructure), one is forced to conclude that the grain size distribution not only has an effect on the plastic response of the polycrystals, but in fact plays a significant and controlling role. Thus far, very few studies have considered the effect of grain size distribution on the mechanical behavior of polycrystals, which raises the question of why the effect of such an important microstructural parameter had until now remained relatively undetected.

Several reasons can be put forth for the evident scarcity of study of this parameter. First and foremost, as discussed in the last chapter, the grain volume distribution is a subtle characteristic of the polycrystalline microstructure, not easily accessed through a two-dimensional examination. Consider, for example, a random two dimensional section through a hypothetical isotropic polycrystal comprised of grains of equal size. On such a section, different grains would appear to be of different size, depending on the plane on which their individual volumes are sectioned. In real polycrystals, superimposed on this variation is the variation in grain size, shape and the curvature of grain faces.[1] Consequently, most common methods of microstructural examination are not suitable for determining the distribution of grain volumes. Added to this is a general lack of awareness, with some notable exceptions, of the possibility of control of grain size distributions through common processing routes such as solidification and thermomechanical treatments.[2] Another, perhaps as important, reason is the complexity and variety of effects associated with the plastic deformation of polycrystals, arising from response to general experimental parameters such as the state of stress, strain rate and temperature, test-specific aspects such as the machine stiffness, the specimen geometry and the ratio of microstructural scale to specimen dimensions, as well as the thermophysical characteristics of the system (which may change during the course of the test). Coupled with these effects is the inherent multi-body nature of the polycrystal response. It is therefore not surprising that there are numerous instances in the literature where the investigation is focused so narrowly on the details of a particular phenomenon that a global view of the polycrystal is not given any particular emphasis. Instead, the thrust is to relate the plastic response to microstructural characteristics most often obtained from two dimensional measurements.

---

[1] The absence of a correlation between the size of grains and their shape as well as the curvature of grain faces (which may be positive, negative or even doubly curved) precludes a measurement of three dimensional microstructural parameters (e.g. the number per unit volume, N_V) from two dimensional measurements. See for example DeHoff [64Deh] and DeHoff and Rhines [68Deh].

In the present investigation, the currently accepted polycrystal deformation theories are reexamined in order to include the effects associated with a variation of grain volumes. It will be shown that the variation in grain volumes control, to a significant extent, the stress and strain distributions in plastically deforming polycrystals, resulting in measurable changes in their yield, work hardening and fracture behavior.

---

[2] The exceptions come from the work of F.N. Rhines and his students and the work of Okazaki and Conrad [72Oka]. See for example the excellent work of Patterson [78Pat] and Rhines and Patterson [82Rhi1] as well as the publication by Rhines et. al [82Rhi2] and the thesis of Liu [84Liu].

As far as the plastic deformation of single phase polycrystals is concerned, the current thinking falls into two broad categories: (a) the so called analytical or polyslip models in which the atomic-level details of the deformation process are ignored, with the focus on the response of each deforming unit of the system under the constraints of stress equilibrium and strain compatibility and (b) the dislocation models in which the macroscopic details of the deformation process are de-emphasized, with the emphasis on atomic-scale mechanisms. A brief review of these models is presented below with the focus on their salient features, together with the main assumptions used. Additionally, the investigations which have attempted to deal with the variation in grain size of polycrystals are described, while a review of the tensile behavior of polycrystalline aluminum is presented in the last section.

3.1.1 Analytical Approach

The so called analytical or "polyslip" approach attempts to predict the deformation of polycrystals from that of single crystals via a consideration of the special constraints imposed on the deforming single crystals in the polycrystal. For an excellent review of the polyslip approach, the reader is referred to the article by Kocks [70Koc].

The main features of the polyslip approach can be illustrated by using the deformation of face centered cubic (fcc) metals. As a class, fcc metals deform plastically by slip on one or more of 12 geometrically equivalent slip systems consisting of the three <110> directions in the four {111} planes. In a single crystal, the number of active slip systems depends on their orientation with respect to the external stress. Thus, if the resolved shear stress is initially highest in one slip system, slip will begin in that system.

If on the other hand the resolved shear stresses are equal in more than one system, then slip will occur simultaneously on some or all of them. In all cases, the shear stresses τ and shear strains γ are related to the external tensile stress σ and the tensile strain ε through the so called "Schmid (resolving) factor," M [31Sch], by:

$$M = \frac{\sigma}{\tau} \text{ and } \gamma = M\varepsilon$$

where $M = 1/\cos\lambda \cos\phi$ and λ and ϕ are the angles between the slip direction and the tensile axis and that between the normal to the slip plane and the tensile axis, respectively.

The deformation of grains in a polycrystal is however constrained by their neighbors. Hence, a grain in a polycrystal can not generally deform by single slip, but must deform in a manner which maintains continuity across the boundary. In other words, any description of the deformation behavior of a single grain in a polycrystal must first begin by assuming an arbitrary strain. In the most general case, such an arbitrary strain can be produced by considering six independent components of the strain tensor. If volume constancy is assumed during plastic deformation (generally a good assumption), then slip on five independent slip systems will satisfy the remaining five conditions necessary for the grains in a polycrystal to deform in any arbitrary manner. Based on such considerations, Taylor [38Tay] was the first to calculate the resolving factor M for grains in a polycrystal. His method was based on the principal of virtual work and can be briefly summarized as follows:

Consider a set of n shears that satisfy the continuity conditions at the grain boundary. The energy expended in producing these shears is a summation of $\tau_S d\gamma_S$ where $d\gamma_S$ is an element of shear strain in the glide system *s* and τ_S is the shear stress which activates the glide. This energy must be equal to the work done by the external uniaxial tensile stress to produce a true strain of $d\varepsilon$. Thus,

$$\sigma d\varepsilon = \sum_{s=1}^{n} \tau_s d\gamma_s \tag{3.1}$$

In the restricted case where τ_S has the same value in every slip system,

$$\sigma d\varepsilon = \tau \sum_{s=1}^{n} \left| d\gamma_s \right| \tag{3.2}$$

which can be rewritten as,

$$\frac{\sigma}{\tau} = \frac{\sum_{s=1}^{n} \left| d\gamma_s \right|}{d\varepsilon} \tag{3.3}$$

Analogous to the single crystal, the resolving factor, *M*, is again defined as σ/τ, which for polycrystals is commonly termed as the "Taylor factor." Taylor further reasoned that *M* can be computed by finding that combination of slips which produces the imposed external strain and gives a minimum value of $\Sigma|d\gamma|$. All other possible combinations of slips (which satisfy the strain continuity condition) would require a higher value of σ. Using an assumption that at any stage of deformation, the hardening value is the same throughout the polycrystal, a numerical value of M can be calculated. For his numerical calculation, Taylor assumed that the strain in each grain is the same as the macroscopic strain for the entire specimen. Using a further postulate that exactly five independent slip systems will operate in each grain and that this set of systems will be one out of 96 irreducible sets in an FCC crystal which gives the lowest value of[3]

$$M = \frac{\Sigma|d\gamma|}{d\varepsilon}$$

Taylor calculated these minimum values of M for 44 orientations of the tensile axis with respect to the crystal orientation. Averaging these values for a quasi-isotropic, FCC polycrystal in uniaxial tension gave a value of $M = 3.04$. Taylor used this analysis to compare the behavior of a polycrystal with that of a single crystal with orientation inside the stereographic triangle. As Kocks [58Koc] pointed out, such a comparison may not be meaningful since a single crystal so oriented will deform predominantly by slip on a single system. Kocks further noted that a polycrystal should more properly be compared

---

[3] It can be shown that if U is taken to be the macroscopic potential energy of the deforming system, then the minimum change in the U is given by,

$$dU_{min} = \frac{1}{2}\sigma_{ij}\left[d\varepsilon^{T} - d\varepsilon^{P}\right]$$

where σ_{ij} is the stress tensor and $d\varepsilon$ is the change in the strain. The superscripts T and P denote the total and plastic contributions. Thus, the maximum plastic work gives the minimum stored energy for a given stress state.

with a single crystal of polyslip[4] orientation: based on slip line examination, such a single crystal was found to deform in a manner similar to a "typical" grain in a polycrystal. In general, the <100> and <111> orientations satisfy this requirement. Specifically for aluminum, the <111> orientation is most suitable [61How] because in the case of the <100> orientation, deformation at higher strains (beyond the first few percent) occurs on two slip systems only. In particular for the <111> orientation, the work of Hosford et al. [60Hos] showed that the deformation of aluminum single crystals at low temperatures (in the range of 4.2 to 77 K) occurs by approximately equal slip on the three favored (<110>) directions.

The Taylor approach can be properly termed as the minimum internal work criterion. Bishop and Hill [51Bis] proposed a method which relied on a maximum external work criterion. Later, the two were shown to be equivalent by Chin and Mammel [69Chi] and Kocks [70Koc]. The Taylor-Bishop-Hill approach is an upper bound analysis in that the constitutive estimates preserve strain compatibility but allow the stress equilibrium to be violated. The approach has found extensive application in the literature, including the prediction of yield loci and deformation textures [65Bun, 65Roe].

One of the important assumptions implicit in this treatment is that the polycrystal deformation is homogeneous. In other words, cases in which strain gradient is significant on the scale of the grain size are excluded.

---

[4] Using the terminology of [61How], the orientation is polyslip when the resolved shear stresses are equal on five or more slip systems and it is multislip if the resolved shear stresses are equal on more than one but less than five slip systems.

The above assumption is not supported by experimental data. For example, the early work of Boas and Hargreaves [48Boa] shows clearly that the strain is distributed inhomogeneously in the polycrystal. As noted by Kocks [70Koc], the individual grains adjacent to any particular grain have (deformation) characteristics of their own, which make the boundary conditions vary along the periphery of the particular grain under consideration. This influence may then fragment the grain into domains of nearly uniform deformation.

In a private communication with Kocks (as quoted in [70Koc]), *M.F. Ashby has considered the possibility that these non-uniformities in deformation contribute directly to the yield strength* and found that this would lead to a yield strength which is related to the square root of the sum of a constant and the inverse of grain size.

In summary, the analytical approach, although extremely useful in predictions of deformation textures, is not particularly suited for examining grain size-flow stress relationships in polycrystals. Nevertheless, the approach provides a valuable starting point for understanding, in particular, the effect of constraints placed on the individual grains in deforming polycrystals. Thus, for example, one may invoke the operation of strictly five slip systems in highly constrained volumes of grains such as those near edges and corners, while relaxing the requirement in less constrained regions such as grain interiors, as well as surface grains. Use of such a differentiation allows for the effect individual grain volumes (and therefore of the grain volume distribution) to be included in the formalism, as discussed in greater detail later.

3.1.2 Dislocation Approach

The dislocation models can be divided broadly into two categories:

(a) those which invoke dislocation pileups and deal primarily with polycrystal behavior at yield and

(b) those which do not invoke dislocation pileups and deal with yield as well as post-yield, i.e. the work hardening behavior

In some instances an approach is also used in which the behavior at yield is modeled and extrapolated to higher strain regimes and vice-versa, while at the other end of the spectrum are those which model the behavior of the polycrystals at the microstrain (microyield) level.

3.1.2.1 Dislocation pileup approach

In this class of models, a significant amount of theoretical work has been carried out in an attempt to understand and explain the role of dislocations in grain size-flow stress relationships, i.e. the well known Hall-Petch relation. The original mechanism proposed by Hall [51Hal] invoked a pileup of dislocations against grain boundaries, as shown in Figure 3.1.

The flow stress, σ, is taken to be that external stress, which, with the help of the pileup, creates a critical stress concentration a certain distance ahead of the pileup. The Hall view was later modified by Cottrell [58Cot] who suggested that the

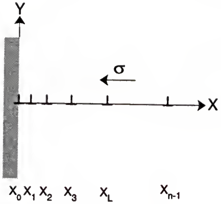

Figure 3.1 Dislocation pile-up against a grain boundary (*xz* plane).

critical stress concentration is that which can unpin a dislocation source near the grain boundary. Petch proposed a similar mechanism [53Pet], with the exception that the critical stress concentration was thought to exist *at* the grain boundary, with yielding commencing when the stress concentration reaches the strength of the grain boundary.

Many theoretical treatments have been devoted to various types of pileups [70Li], including single layer single ended in homogeneous, heterogeneous and anisotropic media [51Esh, 66Cho, 68Kau], single layer double ended [68Hir], circular [67Li], and multiple layer.

Derivation of the Hall-Petch relationship. The derivation given below is based on the analysis of [51Esh, 53Pet, 67Cho, 67Li and 70Li]. As shown in Figure 3.1, consider a pileup of dislocations, all of the same Burgers vector and parallel to the z axis, with xz as the slip plane. At equilibrium, the force exerted on each free (unpinned) dislocation is zero. The equilibrium relation can be written as:

$$\frac{A}{x_i} + \sum_{\substack{j=1 \\ j \neq i}}^{n-1} \frac{A}{x_i - x_j} - \sigma = 0, \quad i = 1, 2, \ldots\ldots, n-1 \tag{3.4}$$

where $A = \mu b/2\pi$ and $\sigma = \sigma_{yz}$ for screw dislocations, and $A = \mu b/2\pi\,(1-\nu)$ and $\sigma = \sigma_{xy}$ for edge dislocations in an isotropic medium of Burgers vector b, shear modulus μ and Poisson's ratio ν. For mixed dislocations in an isotropic medium, similar expressions can be derived, involving the angle between the dislocation line and the Burgers vector. For an anisotropic medium, the expression involves a summation of the contributions from pure edge and pure screw pileups. Following several mathematical steps, it can be shown that the upper limit of the length of the pileup (for a large number of dislocations in the pileup, n) is given by:

$$l = 2nA/\sigma \tag{3.5}$$

The stress concentration σ_{tip} exerted on the pinned dislocation can then be obtained from the external forces exerted on all free dislocations which sum up to $(n-1)\sigma b$. Since the system is at equilibrium, $(\sigma_{tip} - \sigma)b = (n-1)\sigma b$. Thus,

$$\sigma_{tip} = n\sigma \tag{3.6}$$

By assuming that the yield condition is reached when a critical stress, σ_c, is required at the grain boundary in order to propagate the plastic deformation, i.e. $\sigma_{tip} = \sigma_c$, the flow stress-grain size relationship can be derived as follows:

$$n = \frac{\sigma_c}{\sigma}$$

Substituting for n in equation 3.5,

$$l = \frac{2\sigma_c A}{\sigma^2}$$

Solving for σ,

$$\sigma = \sqrt{2\sigma_c A}\, l^{-\frac{1}{2}} \tag{3.7}$$

Adding a possible frictional stress term, σ^*, and *assuming that the maximum length of the pileup is equal to the "grain size,"* the Hall-Petch relation is obtained. Thus,

$$\sigma = \sigma^* + \sqrt{2\sigma_c A}\, l^{-\frac{1}{2}} \tag{3.8}$$

Based on Equation (3.8), if one plots the yield stress as a function of the inverse square root of the "average grain size," with a slope equal to $\sqrt{2\sigma_c A}$ (the Hall-Petch slope, k_p), with an intercept of the "intrinsic" matrix strength. It should be stressed that the maximum length of the dislocation pile-up is replaced by the "average grain size" term in an ad-hock manner. In fact, the linear intercept method commonly used to measure the average grain size really measures the average grain boundary area per unit volume of the polycrystal. The values of A and σ_c depend on the details of the system, i.e. the type of pileup and the material. Typical values of σ_c range from about $\mu/30$ to $\mu/5$. In the literature, most of the details of the deformation process are dealt with by changing the value of k. For example, for the case where the pinned dislocations have a different Burgers vector, the slope is modified by a factor of $\sqrt{m}$ [67Cho], where m is approximately 5 for mild steel.

The first assumption of the above derivation, i.e. yielding takes place through a dislocation pileup mechanism, can not be justified by experiments. For example, no pileups are observed in metals with high stacking fault energy (e.g. Al), while in other instances, dislocations are found to be emitted at the grain boundaries without any evidence of a pileup [64Wor1]. Consequently, non-pileup theories of yielding were developed, as discussed below.

3.1.2.2 Non-pileup approach

The non-pileup theories can be further divided into two categories: (i) work hardening theories and (ii) grain boundary source theories.

Work hardening theories. These theories disregard the pileups and *assume a-priori that there exists a linear relation between the yield (or flow) stress and the square root of dislocation density.* Thus,

$$\sigma = \sigma^* + \alpha\mu b\sqrt{\rho} \tag{3.9}$$

where σ is twice the shear stress on an average slip plane, ρ is the average dislocation density and α is on the order of 4 for iron [62Keh]. The value of α would be different if a different Taylor factor is used [63Wil, 64Smi] and/or a forest dislocation density is used instead of average. The work hardening models further *assume that the average distance of slip of dislocations, χ, is proportional to the grain size, l.* Thus,

$$\chi = \beta l$$

where β is the constant of proportionality. Since the plastic strain is given by: $\varepsilon = \rho b\chi$, the total dislocation density can be calculated by assuming that all the dislocations remain in the system:

$$\rho = \frac{\varepsilon}{b\chi}$$

$$= \frac{\varepsilon}{b\beta l}$$

Substitution in equation 3.9 gives,

$$\sigma = \sigma^* + \alpha\mu b\sqrt{\frac{\varepsilon}{b\beta}}\, l^{-\frac{1}{2}} \tag{3.10}$$

Such an approach has been proposed by many investigators, including Louat (as quoted by [65Mar]), [63Mea] and [63Con1]. Johnson [62Joh] appears to have been the first to suggest that the Hall-Petch type dependence is due to work hardening.

Despite a significant amount of experimental work, direct evidence for the validity of equation 3.10 is lacking, except from the work of Conrad et.al [67Con] for niobium. They showed that, as required by the theory, the flow stress is linear with the square root of strain with a constant intercept and that the dislocation density is linear with strain. On the other hand, many other investigations, particularly those of Carreker and Hibbard for copper [53Car] and aluminum [57Car1] and of Carreker for silver [57Car2] show that the Hall-Petch slope (as calculated from equation 3.10) increases with strain. *These data point to the existence of an additional strain-dependent parameter which controls the overall work hardening behavior of polycrystals.* Other non-linear relations between the average slip distance and grain size have been proposed by Conrad [63Con1] and Conrad and Christ [63Con2]. If correct, these would invalidate the Hall-Petch relationship.

Grain boundary source theories. The original version of this approach was developed by Li [63Li], in which the grain boundaries are assumed to act as dislocation sources. The capacity of the grain boundaries to emit dislocations is assumed to be independent of the grain size, but dependent upon their structure and composition. If l_d is the total length of dislocations emitted per unit area of grain boundary at the time of yielding, then the density of dislocations for a spherical grain of diameter l is given by:

$$\rho = \frac{1}{2}\frac{(\pi l^2 l_d)}{(\frac{1}{6}\pi l^3)}$$

$$= 3l_d / l$$

In the above equation, the factor of *1/2* arises because the grain boundary is shared by two grains. The relation can be generalized by replacing the factor of 3 with a generalized shape factor of K (in which case, the diameter is replaced by a characteristic dimension). Substitution in equation 3.9 gives the Hall-Petch relation:

$$\sigma = \sigma^* + \alpha\mu\mathbf{b}\sqrt{Kl_d}\, l^{-\frac{1}{2}} \tag{3.11}$$

Note that equation 3.11 does not contain a strain term and hence can not be strictly considered as a work hardening theory, however it is classified as such because equation 3.9 is still taken as an established experimental fact. Many studies in the literature have shown that grain boundaries can act as dislocation sources, most notably those of Hornbogen [63Hor], Carrington and McLean [65Car] and Worthington and Smith [64Wor1]. In addition, Suits and Chalmers [61Sui] calculated a relation between the number of yielded grains as a function of stress based on a uniform distribution of sources inside the grains. The experimental observations do not agree with Suits and Chalmers' calculations. Also, it was found that in the early stages of yielding, there are slip lines only on one side of the boundary.

In summary, the formal basis for the Hall-Petch relation presented above shows that the original theoretical treatment has lost much of its utility because of a lack of direct experimental evidence of dislocation pileups. In addition, the non-pileup models are still vague in their details and the major requirements of work hardening model are rarely met. On the other hand, the grain boundary source theories avoid these difficulties by introducing the concept of source density in the grain boundary. However, a direct quantitative determination of grain boundary source density has yet to carried out.

Even if the above shortcomings were to be avoided, the fact still remains that the entire analysis is based on a key extrapolation of the single grain behavior to that of the polycrystal. More specifically, the analysis is developed for a grain of a given characteristic dimension (most commonly called the "diameter") and then applied ad-hoc to the polycrystal as a whole. In doing so, the treatment all but ignores the macroscopic details of polycrystal deformation. Strictly speaking, the extrapolation is valid only for the case where all the grains of the polycrystal are of the same size. Consequently, the strength calculations from such an analysis can be thought of as an upper bound value.

In an interesting addition to the literature on the grain size - flow stress relationship in metals and alloys, Baldwin [58Bal] replotted the flow stress data of various investigators for copper, molybdenum, titanium, mild steel, Al-Mg alloys, brasses (90:10, 85:15 and 70:30) and zirconium versus the inverse cube root of the average grain size. In each case, he showed that the correlation was as good or better than the Hall-

Petch relationship, but offered no theoretical basis for using $(d)^{-1/3}$. Such an analysis reinforces this author's belief that the use of a two-dimensional averaging procedure for measuring microstructural characteristics may mask the true nature of polycrystal deformation.

3.1.3 Size distribution approach

In real polycrystals where a wide variation in grain sizes is commonly encountered, any model of the polycrystal deformation mechanisms must incorporate this size variation. The effect of this microstructural characteristic has, by and large, been ignored in the so called "main-stream" theoretical and experimental treatments of plastic deformation, despite the fact that strain gradients on the scale of grain size as well as regions comprising of several grains have been observed. Thus for example, the work of Essman et al. [68Ess] has shown that plastic deformation of polycrystals begins in the largest grains, while Douthwaite and Evans [73Dou] reported for Fe-Si alloys the presence of isolated plastically deformed grains in an elastic matrix. In his study of creep in aluminum, Connell [73Con] observed that subgrain structure always developed first in the largest grains in the cross section, again indicating a preferential distribution of plastic strain in the polycrystal. Later, direct experimental evidence of inhomogeneous plastic deformation in aluminum was presented by Ellis [80Ell] and by Rhines et al. [81Rhi]. They showed that during deformation by rolling, only about 10% of the volume could be classified as deformed at a reduction in thickness of 10%, while at a 25% reduction, only 37% of the volume showed evidence of deformation. In addition, the number fraction of the grains was smaller than the volume fraction, indicating that the deformed grains must be larger in size than the average grain, as shown in Figure 3.2.

The work of Masui and Takechi [74Mas] appears to be the first one to systematically consider size distribution effects in polycrystal deformation. As discussed below, they derived a relation between the distribution of grain diameters and flow stress in mild steel over a limited strain range. Assuming that over a limited strain range, the stress varied approximately linearly with strain, thus

$$\sigma = \sigma_0(x) + K(x)\varepsilon \tag{3.12}$$

where $\sigma_0(x)$ and $K(x)$ were experimentally determined functions of grain diameter, x, of the form,

$$\sigma_0(x) = A + x^{-\frac{1}{2}} \text{ and}$$

$$K(x) = B + Cx^{-\frac{1}{2}}$$

where A, B and C are constants. Masui and Takechi considered constant stress as well as constant strain models (i.e. maintaining stress equilibrium but violating strain compatibility or maintaining strain compatibility but violating stress equilibrium). For the constant strain case[5] shown schematically in Figure 3.3, consider grains in a specimen

---

[5] Described because of two reasons: (i) the essential judgment of the polyslip models is that it is more important to satisfy strain continuity than stress equilibrium (especially at large strains) [70Koc] and (ii) the constant strain calculations are more tractable and yield results which are numerically very close to the constant stress approach.

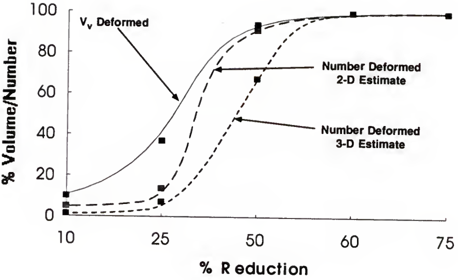

Figure 3.2 Percent of grains deformed (by volume or number) as a function of deformation by rolling. Data of Rhines et. al [81Rhi].

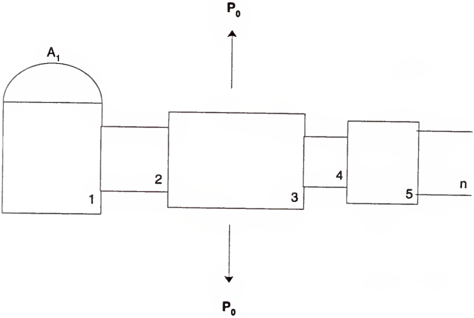

Figure 3.3 Basis of flow stress calculation, constant strain case. Shows grains of areas $A_1 ... A_n$ normal to the tensile axis [74Mas].

cross section with areas of $A_1, A_2, ...A_n$, normal to the tensile axis, subjected to a tensile load of P_0. The load P_0 can be described by equation (3.13) as,

$$P_0 = \sum_{i=1}^{n} \sigma_i A_i \tag{3.13}$$

and the flow stress σ by equation (3.14) as,

$$\sigma = \sum \sigma(x) \frac{x^3 f(x)}{\{\sum x^3 f(x)\}} \tag{3.14}$$

where $\sigma(x) = \sigma_0(x) + K(x)\varepsilon$ and $f(x)$ is the probability density function of grains of diameter x. Using three different probability density functions for the grain diameter distributions (Poisson, Gaussian and Uniform), they showed that the flow stress decreased with increasing standard deviation. Furthermore, the change in the flow stress per unit change in the standard deviation increased with decreasing average grain size.

In a later study, Ghosh and Raj [81Gho] considered the effect of grain size distributions in superplastic deformation of aluminum. Assuming the grain size variation to be represented by a series of triangular distributions with discrete mean sizes, they were able to demonstrate that the stress rise in coarser grains was significantly greater than the finer grains during loading at constant strain rate. Their model reproduced the experimental σ vs. ε behavior of Al and Ti alloys during superplastic deformation extremely well. They concluded that the coarse grains primarily control the transient loading behavior of the alloys and give rise to a transient hardening behavior, resulting in a lower slope of the σ vs. ε curve.

Gokhale and Rhines [83Gok], using preliminary experimental results, showed that the grain volume distribution width influenced the plastic properties of high purity aluminum. Based on these results, it was hypothesized that the plastic response was controlled by the manner in which grains of various sizes actively participated at increasing levels of strain. In the present investigation, the scope of investigation was increased in order to study the plastic response over a wider range of grain volume distribution parameters. As discussed later, this has made it possible to refine and better define the original mechanism proposed by Gokhale and Rhines.

Takimoro and Fujiwara [87Tak] investigated the effect of grain size distribution on the strain hardening exponent and plastic flow of aluminum, copper and 60-40 brass. They reported that the grain size distributions based on two dimensional measurements were well approximated as log-normal and employed a model which calculated the "composite" flow stress of the polycrystals based on a summation of the flow stresses of grains of the polycrystal, weighted on the basis of their probability density in the size distribution. Using a constant strain and constant stress approach similar to [74 Mas] discussed earlier, they concluded that the flow stress increases with a decrease in the median size and decreases with an increase in the standard deviation. An example of their calculation is shown in Figure 3.4, with the flow curves for 60-40 brass for samples with the same median but different distribution widths. It can be seen that the flow stress for the sample with the smaller distribution width is higher than one with the larger width. Also shown are their calculated flow curves. Note that the deviation at small

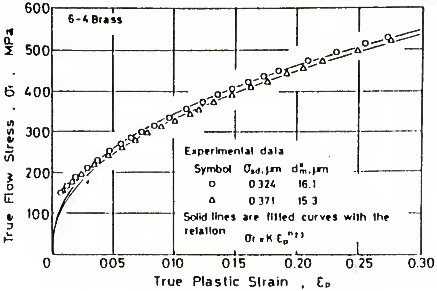

Figure 3.4 Change in the flow stress of 60-40 brass samples with the same median size but different distribution widths. Sample with smaller distribution width has the higher flow curve. Data of [87Tak].

strains between experimental and calculated values arises due to their use of the original Hollomon equation (discussed in the next section), i.e. without taking into account the yield strength.

In a more recent series of publications, Kurzydlowski and coworkers have attempted to describe the effect of grain size variation on plastic response of polycrystals. In the first publication of the series, Kurzydlowski [90Kur] hypothesized based on "intuition"[6] that the flow stress of polycrystals may not only depend on the mean grain size but also on the higher order parameters- for example the standard deviation of the grain sizes. He proposed a model based on a polycrystal comprised of subpolycrystals, with each subpolycrystal made up of grains of equal size. The strength of the polycrystal was then derived from a weighted average of the strengths of the subpolycrystals, calculated on the basis of the Hall-Petch relationship. Based on these calculations, [90Kur] concluded that the strength of the polycrystals decreased with increasing grain size distribution width. Rather surprisingly, his calculations also indicated that a polycrystal with highly inhomogeneous deformation would require a higher flow stress than one with a homogeneous deformation, when compared at the same average grain size and grain size distribution width. This type of suggested behavior appears to be related more to the particular assumptions used rather than the physical realities of polycrystal deformation: one cannot, for example, assume the same grain size distribution width but two different deformation mechanisms, since one controls the other. Kurzydlowski explained this result of the model on the basis of the greater work hardening in larger grains.[7] As discussed later, the work hardening rate of the larger crystals in the polycrystal is indeed higher during initial deformation. However, their net contribution to the flow stress per unit volume always lags behind that of the finer crystals. Kurzydlowski and Bucki [93Kur] also explored the effect of grain size distribution in polycrystals made from sintered stainless steel powder mixtures. They noted that the differences in the distribution function resulted in a systematic deviation in the hardness from the Hall-Petch relation and that polycrystals with a higher diversity of grain sizes (as measured by a grain area coefficient of variation) exhibited hardnesses lower than the Hall-Petch prediction.

---

[6] He did not however quote the earlier work of [74Mas], [81Gho], [83Gok] and [87Tak].

In summary, it is clear that the grain size distribution exerts an influence on the plastic behavior of single phase polycrystals. The direct experimental evidence of the extent and nature of this influence for aluminum is presented in the results section of this chapter.

3.1.4 Summary of aluminum tensile properties

Room temperature tests. In recent years, a number of investigators have reported the Hall-Petch constants for aluminum tested at room temperature, with the initial strain rate ranging from 0.3 to $8.3\text{x}10^{-4}$ s^{-1}. Their data for friction stress (Hall-Petch intercept) and Hall-Petch slope are summarized in Figures 3.5(a) and 3.5(b), respectively. It can be seen that there is a wide discrepancy between the values reported by the various investigators, with the intercept ranging from 3 to 18 MPa and the slope from 0.01 to

---

[7] Kurzydlowski does note that the result is ambiguous.

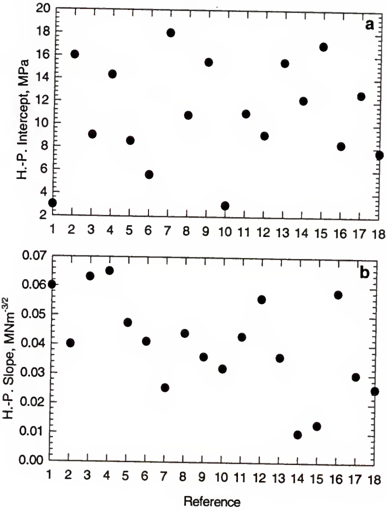

Figure 3.5 Room temperature data on pure pure aluminum. Literature sources are numbered from 1 to 18. (a) Hall-Petch intercepts and (b) Hall-Petch slopes. Literature sources: 1-[64Hul], 2-[69Han1], 3-[73Fuj], 4-[73Tho], 5-[75Kle], 6-[77Han(a)], 7-[77Han(b)], 8-[81Wyr(a)], 9-[81Wyr(b)], 10-[83Alh(a)], 11-[83Alh(b)], 12-[83Wyr(a)], 13-[83Wyr(b)], 14-[86Wyr(a)], 15-[86Wyr(b)], 16-[86Wyr(c)], 17-[86Wyr(d)], 18-[87Dol].

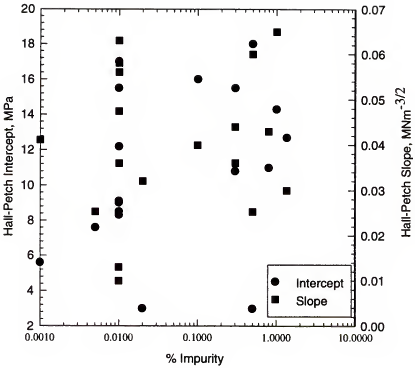

Figure 3.6 Hall-Petch constants as a function of impurity content from literature sources listed in Figure 3.5(a).

0.065 MNm$^{-3/2}$. The main differences between the various investigations came from the material purity and the thermomechanical treatments. An effort to explain the differences on the basis of purity failed, as illustrated in Figure 3.6. The figure shows the intercept and slope as a function of the reported impurity content of the material, plotted on a logarithmic scale so as to resolve the small differences in the impurity content. It can be seen that there is no sensible correlation between the Hall-Petch constants and the material impurity. Consequently, the only factor to which the observed scatter can be attributed is the thermomechanical history of the samples, which, it may be recalled from Chapter 2, directly alters the parameters of the grain volume distribution. This analysis thus supplies another indication that the grain volume distribution affects the mechanical behavior of aluminum. A calculation of the grain volume distribution widths from the reported thermomechanical histories of the samples and their correlation with the measured yield strengths was not possible due to insufficient information.

Tests at 77 K. In comparison with the volume of data available for room temperature, those at 77 K are limited. In their early work, Carreker and Hibbard [57Car1] determined the tensile behavior of two purities of aluminum (99.975 and 99.987%) as a function of temperature, strain rate and grain size. Their thermomechanical treatment consisted of approximately 99.64% reduction in area prior to recrystallization and annealing (to obtain a grain size range). This treatment produced a material with a strong <111> fiber texture with some <100> fiber present. At 77 K, they reported yield strengths around 38 and 34 MPa, and strain hardening exponents of 0.4 to 0.45 and 0.41 to 0.45 for the two purities, respectively. They noted that at the various temperatures used, the yield strengths were not a sensible function of the grain size, but that a "fortuitous" linear dependence was observed at room temperature on a log-log plot of yield vs. grain size in the true strain range of 0.005 to 0.05. Since the thermomechanical treatment used by [57Car] was identical for all samples, one can assume that the grain volume distribution width for all samples was the same. Furthermore, because of the high level of pre-recrystallization deformation, the width is likely to be low, on the order of 0.8.

Around the same time period, Trozera et.al. [57Tro] investigated the effect of strain rate and temperature on the plastic deformation of high purity aluminum (99.997%). As far as can be determined, their samples were given identical thermomechanical treatments (corresponding to a constant value of grain volume distribution width). They reported a yield strength of 14.13 MPa at 77 K and also at 77 K, a very small dependence of the flow stress on strain rate in the range $1.9\text{x}10^{-3}$ to $4.7\text{x}10^{-5}\ \text{s}^{-1}$. Their data showed excellent reproducibility of flow curves for samples tested over a wide range of strain rates and temperatures. Thus, combining the effect of strain rate and temperature as: $Z = \dot{\varepsilon}\ e^{-\Delta H/RT}$, the flow curves of various samples could be made to superimpose at identical values of Z. Such reproducibility is a rarity rather than the rule in investigations dealing with plastic deformation, and was perhaps realized only because the superimposed effects of grain size and size distribution were avoided by the experimental procedure employed.

In a more recent study, Al-Haidary et.al. [83Alh] investigated the plastic behavior of two purities of Al (99.2 and 99.98%) as a function of grain size. They tested all samples at a strain rate of $4\text{x}10^{-4}\ \text{s}^{-1}$ at 77 K. They however produced their grain sizes by employing varying thermomechanical treatments. For example, for the lower purity material, the finest grain sizes were obtained by using a lateral compression of 30%, followed by cold rolling to a total deformation of 90% and recrystallization at 400°C, whereas the coarse grained material was obtained by using a 4% critical strain, followed by annealing at 620°C. Based on the data presented in the last chapter, the latter treatment must most certainly have produced a material with a very wide grain volume distribution width. They reported intrinsic yield strengths (Hall-Petch intercepts) of 24 and 15.6 MPa respectively, for the low and high purity grades, and an identical Hall-Petch slope of 1.36 $N/mm^{3/2}$.

In summary, the flow stress-grain size relationship for aluminum appears to broadly follow the Hall-Petch equation at room temperature, so long as one replaces (1/2) by "n" where n varies over a wide range (Figures 3.5(a) and 3.5(b)), but exhibits striking differences when the data of various investigators are compared. On the other hand, the Hall-Petch relationship does not hold as strongly at lower temperatures. Analysis of the data from various investigators also reinforces the belief that the differences in the data are most likely related to the differences in the thermomechanical history of the samples, and by inference, the grain volume distribution width.

3.2 Experimental Procedure

As noted earlier, the main thrust of the present investigation was to test samples with (nominally) the same grain boundary area per unit volume (S_v) but varying GVD widths ($\ln\sigma_g$'s) under uniaxial tensile stress. In order to obtain these microstructural conditions, a series of thermomechanical treatments, i.e. one or more deformation-recrystallization steps to set the $\ln\sigma_g$ followed by an annealing step (for an appropriate length of time) to set the S_v, were employed. The first part of the procedure was described in detail in Chapter 2. Concerning the annealing step, it may be recalled that the findings of Rhines and Patterson [82Rhi1] and Okazaki and Conrad [72Oka] indicated that the $\ln\sigma_g$ established through the final deformation-recrystallization step remains essentially unchanged during subsequent grain growth. As described later, this finding was reconfirmed in the present investigation.

Using this strategy, for each level of $\ln\sigma_g$, tensile test specimens with two S_v's, 4.45 and 8 mm^2/mm^3 (corresponding to mean intercept grain sizes of 0.45 and 0.25 mm, respectively), were produced. The decision to use these S_v's was based on the following considerations: (a) the grain sizes were far enough apart in magnitude to reveal any Hall-Petch type effect, (b) at these sizes, less than 10% of the grains constituted surface grains, thus minimizing the influence of free-surface related effects [57Iak] on mechanical property values, (c) the determination of the GVD via the grain separation procedure was experimentally found to be more reliable for coarse-grained samples and (d) these S_v's could be produced using only those deformation steps which minimized the development of a preferred rolling texture [59Ric][8].

---

[8] Samples used in the present investigation were analyzed for texture-modified yield strengths. It was found that texture was not a significant factor in controlling the yield strengths of these samples. In fact, the crystallographic orientation distribution function was found to be random [92Mar].

The deformation-recrystallization sequences used to produce the required $\ln\sigma_g$ levels were described in the last chapter. Subsequent isothermal annealing to attain the desired S_v levels presented two additional complications: (a) the starting S_v for each recrystallized block was a function of the prior deformation history and (b) for each deformation-recrystallization history (and therefore each $\ln\sigma_g$) the rate of grain growth is dependent on the $\ln\sigma_g$ (increases with increasing $\ln\sigma_g$) [82Rhi1]. Consequently, the steady state grain growth for each level of $\ln\sigma_g$ was determined experimentally.

The recrystallization temperatures were selected so as to yield an equiaxed and homogeneous microstructure, resulting in the following recrystallization conditions for the S.P. and H.P. series:

S.P. : Recirculating air furnace, 450 ± 1° C

H.P. : Neutral salt bath furnace, 510 ± 2° C

In each case, a test block of Al equipped with surface and center thermocouples and of dimensions similar to the experimental blocks (approximately 16 cm X 7 cm X 2 cm) was first used to check the heating characteristics. It was found that the temperature difference in the two regions became negligible after approximately three minutes. Heating for an additional two minutes produced the desired recrystallized microstructures.

Following the recrystallization treatment, each experimental block was sawed as shown in Figure 3.7. Referring to Figure 3.7, of the six samples cut from one end, one was prepared metallographically on two mutually perpendicular planes (parallel and normal to the rolling plane) as indicated by the shading. Examination of the microstructure and comparison of S_v values from the two planes of polish confirmed that for each block the microstructure was indeed equiaxed and homogeneous.

For metallographic examination, the samples were prepared using standard mechanical grinding/polishing steps, the final step being 3200 mesh emery/soap slurry on a microcloth. The mechanical preparation was followed by the following electropolishing/etching technique developed by Connell [72Con]:

Electrolyte: 8.2 cc HF, 4.5 g Boric acid, 250 cc distilled water
Cathode: Cl^- free graphite
Distance: 2.5 cm
Agitation: without cavitation
Voltage: 20 V O.C.
Time: 30 to 40 s for polishing, additional 15 to 25 s for etching

It was found that the polishing/etching conditions were not very sensitive to the anode/cathode area ratio. The polishing conditions described above produced and excellent mirror surface finish free of strain, while the etching produced an anodic film on the surface which gave rise to a brightly colored grain contrast under polarized light with a quarter wavelength filter. Literature indicated that such anodic films grow epitaxially on Al [63Doh, 81Mat]. Previous work [80Ell] has shown that this method can be used successfully to not only reveal the deformed microstructures, but also to distinguish between undeformed and slightly deformed grains. This is illustrated in Figures 3.8(a) and 3.8(b), for an annealed and an 25% compressed sample, respectively. It can also be seen that the grain boundaries are revealed unambiguously, which is necessary for an accurate measurement of the S_v.

The remaining five samples from this sawed section were annealed at 450 and 510°C for the S.P. and H.P. grades, respectively, for times ranging from 15 to 120 minutes (15, 30, 45, 60 and 120). Smaller annealing times were not considered because only the steady state grain growth rate was of interest here. Note that due to the smaller dimensions of these samples, the entire sample attained the annealing temperature in less than one minute; the annealing times listed are after the initial heat-up period.

The annealed samples were prepared metallographically on a plane parallel to the rolling plane, as shown by the shading in Figure 3.7. For each sample, S_v was measured to an accuracy of ±5% using the standard linear intercept method [68Sch]. No special sample design was needed because the structures were uniform and isotropic.

As shown in Figure 3.7, three tensile test samples were prepared from each block. Using the grain growth parameters for each deformation and purity level, two of these

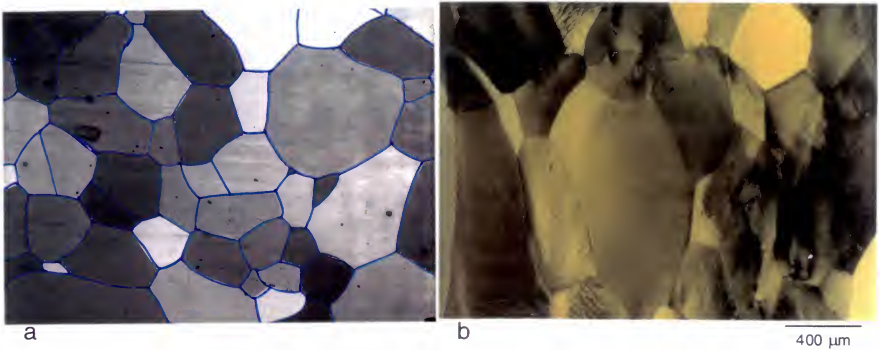

Figure 3.8 Microstructure of aluminum samples: (a) annealed and (b) 25% compressed.

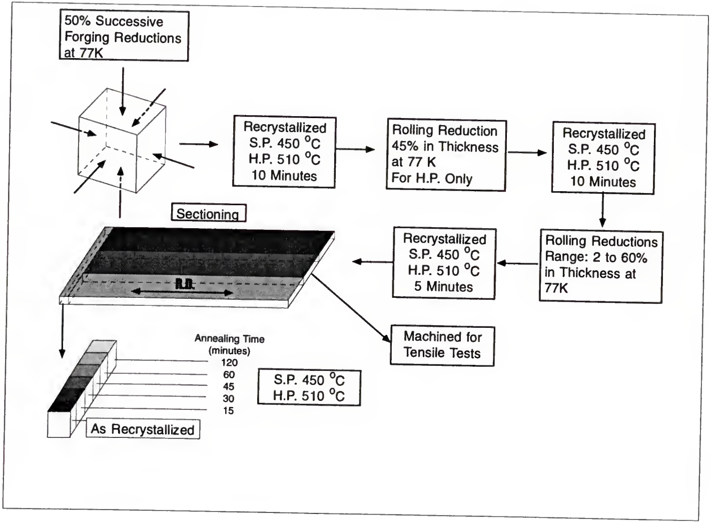
50% Successive Forging Reductions at 77K
Recrystallized S.P. 450 °C H.P. 510 °C 10 Minutes
Rolling Reduction 45% in Thickness at 77 K For H.P. Only
Recrystallized S.P. 450 °C H.P. 510 °C 10 Minutes
Rolling Reductions Range: 2 to 60% in Thickness at 77K
Recrystallized S.P. 450 °C H.P. 510 °C 5 Minutes
Sectioning
R.D.
Machined for Tensile Tests
Annealing Time (minutes)
120
60
45
30
15
S.P. 450 °C H.P. 510 °C
As Recrystallized

Figure 3.7 Thermomechanical schedule and sectioning of experimental samples.

samples were annealed until they had attained an S_v of 8 mm^2/mm^3 (denoted as $S_v(1)$) and the remaining sample until it had attained an S_V of 4.45 mm^2/mm^3 (denoted as $S_v(2)$).

After annealing, the samples were machined to produce standard tensile test bars according to ASTM Specification E8-80a [84ASTM1] (gage length 5.08 cm and gage diameter 1.27 cm). All the test pieces had their tensile axes parallel to the rolling direction. During machining, the pieces were cooled intermittently in liquid nitrogen to minimize deformation during machining. In order to reduce the effect of surface irregularities, the machined gage lengths were lightly polished using 3200 mesh emery followed by electrolytic polishing using the procedure described above and cleaned in acetone. The gage diameters were measured on an optical comparator for use in the strength calculations and also to ensure that the test pieces conformed to the ASTM specification.

All tensile testing was performed on a floor model C/D Instron Universal Testing machine at an initial strain rate of $4.17X10^{-4}$ $s.^{-1}$ The test temperature was maintained at 77 K by using a special jig which allowed the test pieces and grips to be immersed in liquid nitrogen during the test. Use of the liquid nitrogen bath provided a uniform test temperature for all the samples and also avoided any dynamic recovery effects during testing.

Following the tensile tests (which were carried out to fracture), metallographic samples were prepared from the grip portions and used for S_v measurements. These are average S_v values reported for each sample. It was found that, with minor variations, the average S_v was that calculated from the grain growth data. In addition, the GVD was

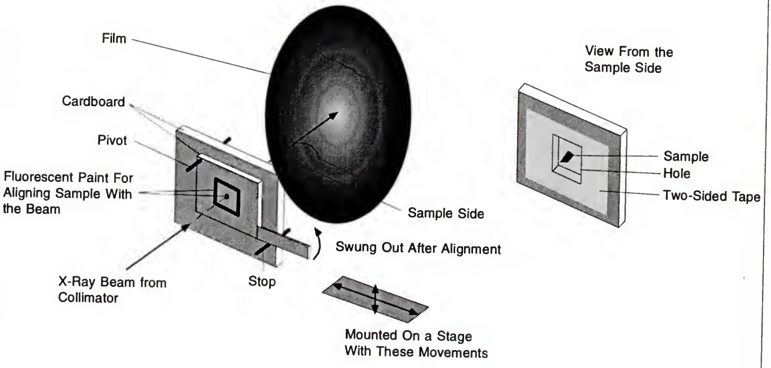
Film
Cardboard
Pivot
Fluorescent Paint For Aligning Sample With the Beam
X-Ray Beam from Collimator
Stop
Sample Side
Swung Out After Alignment
Mounted On a Stage With These Movements
View From the Sample Side
Sample
Hole
Two-Sided Tape

Mo white radiation. Tube voltage: 40 kV. Tube current: 10 mA. Exposure time: 15 minutes. Sample to film distance: 5 cm. Transmission Laue.

Figure 3.9 Experimental arrangement for obtaining transmission Laue patterns of individual grains.

remeasured from the grip portions of three samples of each grade of aluminum annealed to the nominal average S_v value of 8 mm^2/mm^3 (two from the extremes of the $\ln\sigma_g$ range and one from the middle of the range). In each case, the reported constancy of $\ln\sigma_g$ during steady state grain growth [72Oka, 78Pat, 82Rhi1] was reconfirmed.

In order obtain a qualitative correlation between grain volumes and the amount of strain in grains of plastically deformed polycrystals, the following procedure was developed: using the grip portion of one of the tensile samples, a compression sample was machined using ASTM Specification E-9 [84ASTM2]. The sample was compressed at 77 K to an 8% reduction in height at an initial strain rate of $4.17X10^{-4}$ $s.^{-1}$ Following the test, the grains from the central portion of the sample were separated using the procedure described in Chapter 2. For this grain separation, the lowest possible temperature (50°C) was used to minimize recovery in the deformed polycrystal. Immediately following the separation, the grains were kept cool in a freezer until subjected to X-ray analysis. For grains widely differing in volume, transmission Laue patterns were obtained using the scheme shown in Figure 3.9. The results of this procedure are included in the next chapter.

3.3 Results and Discussion

The results of the tensile tests are presented using the following division:

(a) Yield Behavior,

(b) Post-Yield Flow Behavior,

(c) True Stress at Point of Instability and Uniform Strain and

(d) True Fracture Strain

In each part, there are four sets of tensile test data consisting of one series of samples each: S.P.S_v(1), S.P.S_v(2), H.P.S_v(1) and H.P.S_v(2), where the designations are as before.

3.3.1 Background

3.3.1.1 True stress and true strain

The load elongation values obtained for each sample were first converted to engineering stress-strain values and subsequently to true stress-true strain values using the following standard relations [85Die]:

$$S = \frac{P_i}{A_0} \tag{3.15}$$

$$e = \frac{\Delta L}{L_0} \tag{3.16}$$

$$\sigma_t = \frac{P}{A_i} \tag{3.17}$$

where S is the engineering stress, P is the measured load, A_0 is the initial area of cross section, e is the engineering strain, ΔL and L_0 are the change in length and initial length (of the gage section), respectively, σ_t is the true stress and A_i is the instantaneous area of cross section. The true strain is calculated by assuming volume constancy ($A_iL_i = A_oL_o$) during plastic deformation, thus:

$$A_i = \frac{A_0L_0}{L_i} \tag{3.18}$$

Substituting for A_i in equation 3.17,

$$\sigma_t = \frac{P_iL_i}{A_0L_0} \tag{3.19}$$

Since $L_i = \Delta L + L_0$,

$$\begin{aligned}\sigma_t &= \frac{P_i}{A_0}\left[\frac{L_0 + \Delta L}{L_0}\right] \\ &= S[1+e]\end{aligned} \tag{3.20}$$

The true strain ε_t is given by,

$$\begin{aligned}\varepsilon_t &= \int_{L_0}^{L} \frac{dL}{L} \\ &= \ln\left[\frac{L}{L_0}\right] \\ &= \ln[1+e]\end{aligned} \tag{3.21}$$

3.3.1.2 The yield strength

The stress at which plastic deformation or yielding is observed depends on the sensitivity of the measurement. While the true elastic limit must be determined from microstrain measurements, the yield strength on the other hand is defined as the stress required to produce a small specified amount of plastic deformation, usually 0.002. The stress may be measured either from engineering stress-strain curves or from true stress-strain curves without introducing any appreciable error. This is because at the small strain limit, the engineering and true strains or nearly equal, as shown below:

for e = 0.02% or 0.002,

$$\begin{aligned}\varepsilon_t &= \ln(1 + e)\\ &= \ln(1 + 0.002)\\ &= 0.001998\end{aligned}$$

In the present investigation, the yield strengths were measured at $\varepsilon_t = 0.002$.

3.3.1.3 Stress at uniform strain limit

For FCC metals, macroscopic necking generally manifests itself as the point of maximum load, defined by the condition: dP = 0, which is also commonly termed as the instability criterion since the majority of deformation is concentrated in the neck region beyond this point. Using this criterion and invoking volume constancy during plastic deformation, a simple relationship between the work hardening ($d\sigma_t/d\varepsilon_t$) and the true stress (σ_t) can be obtained [73Ree]:

$$P = \sigma_t A$$

$$\begin{aligned}dP &= \sigma_t\, dA + A\, d\sigma_t\\ &= 0\end{aligned}$$

From the volume constancy relationship,

$$\begin{aligned}dL/L &= -(dA/A)\\ &= d\varepsilon \qquad (3.22)\end{aligned}$$

Substituting for (dA/A) from the instability criterion,

$$d\sigma_t/d\varepsilon_t = \sigma_t \tag{3.23}$$

The point of intersection of the σ_t-ε_t and $(d\sigma_t/d\varepsilon_t)$-$\varepsilon_t$ curves is thus taken as the limit of true uniform strain (ε_u).

3.3.1.4 True fracture strain

The true fracture strain is defined as the maximum strain that the material can withstand before fracture and involves the measurement of the specimen cross section at the plane of fracture. Since most high ductility metals do not fracture on a single plane, the measurement is difficult to perform with accuracy and generally involves a simplifying assumption of single plane of fracture. The true fracture strain is given by: $\varepsilon_f = \ln(A_0/A_f)$, where A_0 and A_f are the original and final specimen cross section areas, respectively.

3.3.2 Results

3.3.2.1 The yield behavior

The yield strength (Y.S.) was measured from the σ_t-ε_t plots at 0.2% strain offset ($\varepsilon_t = 0.002$). The measured values are tabulated for the four sets of data (40 samples) in Tables 3.1 to 3.4, along with the $\ln\sigma_g$ value for each sample. These data are plotted in Figures 3.10(a) and 3.10(b) for the S.P. and H.P. grades, respectively, while a combined

Table 3.1

Grain volume distribution width and yield strength of S.P. $S_v(1)$ samples. The sample identification denotes the purity, the nominal S_v level and the sample and replicate numbers.

Sample	$\ln\sigma_g$	Y. S. (MPa)
SP(1)1-1	1.21	28.31
SP(1)1-2	1.21	28.18
SP(1)2-1	1.28	27.84
SP(1)2-2	1.28	27.55
SP(1)3-1	1.35	26.23
SP(1)3-2	1.35	25.93
SP(1)4-1	1.78	23.31
SP(1)4-2	1.78	23.62
SP(1)5-1	2.23	22.89
SP(1)5-2	2.23	23.11
SP(1)6-1	2.79	22.09
SP(1)6-2	2.79	22.62

Table 3.2

Grain volume distribution width and yield strength of S.P. $S_v(2)$ samples. The sample identification denotes the purity, the nominal S_v level and the sample numbers. No replicates tested for the coarser grain size samples. See experimental procedure for explanation.

Sample	$\ln\sigma_g$	Y. S. (MPa)
SP(2)1-1	1.21	27.64
SP(2)2-1	1.28	27.21
SP(2)3-1	1.35	25.55
SP(2)4-1	1.78	23.86
SP(2)5-1	2.23	23.04
SP(2)6-1	2.79	22.81

Table 3.3
Grain volume distribution width and yield strength of H.P. $S_v(1)$ samples. The sample identification denotes the purity, the nominal S_v level and the sample and replicate numbers.
*Indicates that no replicates were tested for these samples. The replicate tensile bars were deformed during machining and therefore discarded.

Sample	$\ln\sigma_g$	Y. S. (MPa)
HP(1)1-1	1.01	37.33
HP(1)1-2	1.01	38.42
HP(1)1-3	1.01	38.24
HP(1)2-1	1.13	37.02
HP(1)2-2	1.13	36.87
HP(1)3-1	1.15	35.75
HP(1)3-2	1.15	35.29
HP(1)4-1*	1.17	34.65
HP(1)5-1*	1.22	34.99
HP(1)6-1	1.25	34.40
HP(1)6-2	1.25	34.08
HP(1)7-1*	1.31	33.27
HP(1)8-1	1.33	31.12
HP(1)8-2	1.33	32.04

Table 3.4

Grain volume distribution width and yield strength of H.P. $S_v(2)$ samples. The sample identification denotes the purity, the nominal S_v level and the sample numbers. No replicates tested for the coarser grain size samples. See experimental procedure for explanation.

Sample	$\ln\sigma_g$	Y. S. (MPa)
HP(2)1-1	1.01	37.00
HP(2)2-1	1.13	34.60
HP(2)3-1	1.15	36.07
HP(2)4-1	1.17	35.12
HP(2)5-1	1.22	35.81
HP(2)6-1	1.25	34.00
HP(2)7-1	1.31	33.64
HP(2)8-1	1.33	31.29

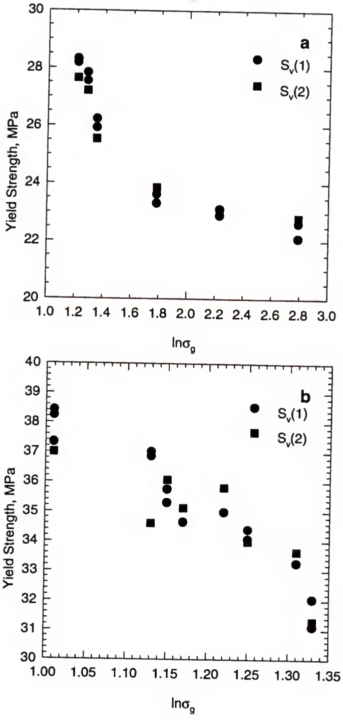

Figure 3.10 Yield strength as a function of the grain volume distribution width for (a) S.P. series and (b) H.P. series. Data for two S_v levels.

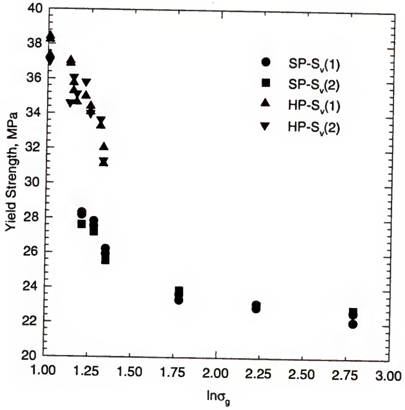

Figure 3.11 Comparison of yield strengths of S.P. and H.P. series as a function of the grain volume distribution width at two S_v levels.

plot of all data is shown in Figure 3.11. Note that each of these plots includes data for the two average S_v (mean intercept "grain size") levels. From these plots, two aspects of the correlation between the Y.S. and $\ln\sigma_g$ are immediately apparent:

(a) there is no significant difference between the yield strengths of samples with the same $\ln\sigma_g$ but two levels of S_v, and

(b) the yield strengths are inversely related to $\ln\sigma_g$.

In order to further investigate the correlation between $\ln\sigma_g$ and Y.S., a simple linearization procedure was sought. It was found that the data could be satisfactorily linearized by expanding the $\ln\sigma_g$ range, done by plotting the Y.S. values against inverse square of $\ln\sigma_g$. The procedure expands the range by about a factor of 3: the original range of approximately 1 to 3 (i.e. factor of 3) changes to 1 to 0.1 (i.e. factor of 10). The plot of Y.S. for both series and S_v levels as a function of $(\ln\sigma_g)^{-2}$ is shown in Figure 3.12. It can be seen that the data fall in two distinct groups, one for each series, independent of the mean intercept grain size. Also, for each group, there is a strong linear correlation of the form:

$$\sigma_y = \sigma_w + k_w[\ln\sigma_g]^{-2} \tag{3.24}$$

where σ_y is the yield strength at 0.2% ε_t and σ_w and k_W are constants whose subscripts indicate that their values were derived from a grain volume distribution dependent relationship. Values of the constants for each series are summarized below:

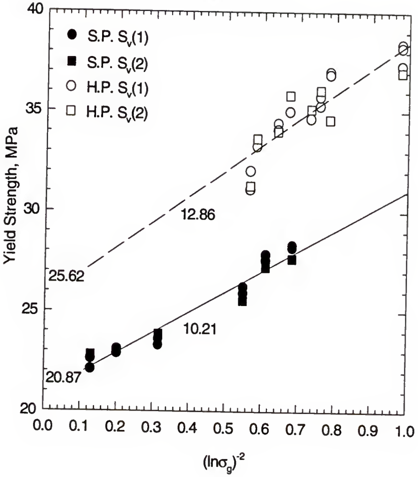

Figure 3.12 Linear dependence of the yield strength on the inverse square of the grain volume distribution width. Data for both S.P. and H.P. purities of aluminum at two S_v levels.

Series	σ_w (MPa)	k_W (MPa)
S.P.	20.87 ± 0.6	10.21 ± 1.2
H.P.	25.62 ± 2.3	12.86 ± 3.0

It can be seen that the intercepts are significantly different at a 95% confidence level while the confidence intervals for the slopes overlap; the lines themselves describe the data well. One of the advantages of the above representation of the data is that the constants have a physical significance because the intercepts represent distribution-independent (intrinsic) yield strengths for the two purities of aluminum.[9] It is therefore not surprising that the material of lower purity shows a higher yield strength. Also, the values reported here compare very well with the range reported in the literature of 18 to 28 MPa for polycrystals, but are somewhat higher than that reported (14 MPa) for pure aluminum single crystals tested at 77 K in a polyslip orientation [60Hos].

The slopes represent the magnitude of change in structural response due to the presence of grain boundaries. However, it must be stressed that such response modification arises not simply because of grain boundaries, but in an important way on the manner in which they are distributed in the microstructure. It may be recalled that the two groups of data comprise of two levels of S_v each, which show no significant difference in their strength levels at constant $\ln\sigma_g$. The difference in the two slopes, if taken to be related to the purity difference in the respective grades, suggest to a moderate extent that the lower purity material is more sensitive to $\ln\sigma_g$ changes, however, no definite conclusion can be drawn on the basis of these data.

---

[9] For a single crystal, the grain volume distribution width is undefined: it can be taken either as zero or infinite. In either case, the extrapolation of $[\ln\sigma_g]^{-2}$ to zero may be taken to represent physically the properties of a single crystal.

At the low plastic strain (0.002) of σ_y, the data from the two purities can be combined without regard to the difference in their respective slopes. This is shown in Figure 3.13 by modifying the σ_y of S.P grade as $\sigma_y(S.P.)_M = \sigma_y(S.P.) + \{\sigma_0(H.P.)-\sigma_0(S.P.)\}$. It can be seen that all the data (four sets) can be represented by a single straight line with a intercept and slope of 24.8 and 13.5 MPa, respectively. As discussed below this correlation can be used to compare the behavior of the samples in strain regimes where work hardening becomes significant.

The above data represent the first direct experimental proof that the yield of single phase polycrystals depends on the grain volume distribution width.

This does not necessarily invalidate the Hall-Petch (H-P) relationship if two specific constraints are invoked: (i) when the GVD width is narrow, i.e. less than unity and (ii) when the behavior is compared at constant GVD width. Also, even for the present samples, an H-P type analysis can be applied fruitfully to further understand the details of the deformation mechanisms. Such an analysis consists of considering the grain boundary area in the microstructure selected on the basis of grain volume-controlled distribution of deformation, and is presented in detail in the next chapter.

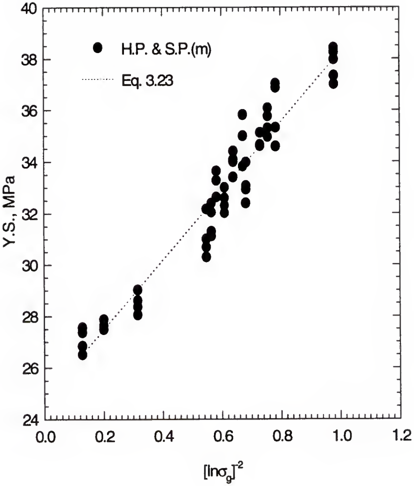

Figure 3.13 Plot of yield strength as a function of the inverse square of the grain volume distribution width. Combined data of S.P. and H.P. purities. Data of S.P. modified (see text). No distinction made on the basis of S_v level.

3.3.2.2 Post yield flow behavior

The true stress - true strain curves for the S.P. and H.P. series at the two S_v levels are shown in Figures 3.14(a) to 3.14(d), respectively. In these plots, the data for samples with the same distribution width were averaged. In engineering terms, these flow curves clearly show that with an increasing grain volume distribution width, the tensile properties degrade.

The tensile flow characteristics of polycrystals are generally analyzed through the use of empirical equations which relate the true stress to true strain. The most common relation is that due to Hollomon [45Hol] who first proposed an equation of the form:

$$\sigma_t = K_0 \varepsilon_t^{n_0} \tag{3.25}$$

where σ_t is the true stress, ε_t is the true strain and K_0 and n_0 are commonly termed as strength coefficient and strain hardening exponent, respectively. The Hollomon equation is valid only beyond yield since it forces the stress-strain curve through the origin without regard to the elastic region. According to Garde and Reed-Hill [75Gar], the Hollomon equation may be modified to include the yield strength. In this case, the plastic portion of the flow curve is still described by the Hollomon equation, while the total flow curve (i.e. including yield) is described by what is termed as the modified Hollomon or Ludwig (as quoted in Garde and Reed-Hill) equation of the form:

$$\sigma_t = \sigma_y + K\varepsilon_t^n \tag{3.26}$$

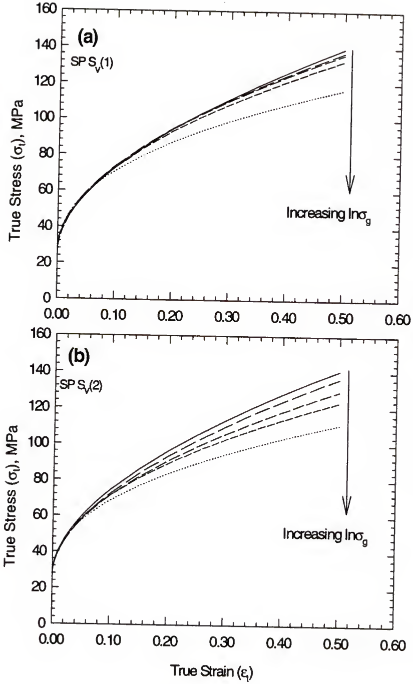

Figure 3.14 True stress - true strain curves for (a) S.P. $S_v(1)$ and (b) S.P. $S_v(2)$. Data for samples with the same distribution width are averaged.

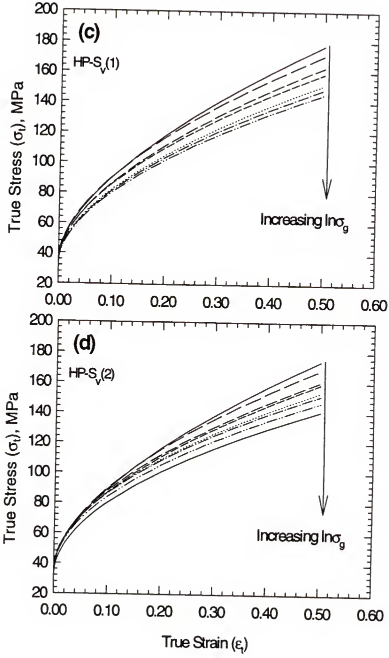

Figure 3.14(continued) (c) H.P. $S_V(1)$ and (d) H.P. $S_V(2)$. Data for samples with the same grain volume distribution width are averaged.

where the various terms have the same meaning as before.

The constants of the Ludwig equation can be obtained from experimental stress-strain data in two ways:

(i) By plotting the logarithm of the slope of the true stress-true strain curve against the logarithm of the true strain. Thus, differentiating equation 3.26 and taking logarithms of both sides,

$$\ln\left(\frac{d\sigma_t}{d\varepsilon_t}\right) = \ln(Kn) + (n-1)\ln(\varepsilon_t) \tag{3.27}$$

the values of K and n can then be obtained from a the slope and intercept of the plot of $\ln(d\sigma_t/d\varepsilon_t)$ vs $\ln(\varepsilon_t)$. The derivative $\ln(d\sigma_t/d\varepsilon_t)$ is however extremely sensitive to the accuracy with which the values are read off the curve. This method is therefore not preferred, the second one given below being more desirable.

(ii) Redefine the origin at σ_y and plot the logarithm of true strain against the logarithm of true stress.

This method was adopted in the present investigation as follows: the σ_t-ε_t curves were digitized in the plastic region beyond yield to obtain 50 points at regular strain intervals. The data were plotted as $\ln(\sigma_t-\sigma_y)$ vs $\ln(\varepsilon_t)$. In each case, a straight line gave the best fit with the correlation coefficients never less than 0.9, most being greater than 0.95. The intercept of the line gave the ln(K) value, the slope being n. It should be noted that because of the number of data points utilized, the values of the constants were not affected by any slight errors in digitizing the data.

The values of K and n, along with the $\ln\sigma_g$ values of the samples are summarized in Tables 3.5 to 3.8. The K and n data are plotted [both S.P. and H.P., $S_v(1)$ and $S_v(2)$] in Figures 3.15 and 3.16, respectively. It can be seen that there is a distinct monotonic decrease as a function of the $\ln\sigma_g$. These values indicate that the work hardening characteristics of the polycrystals are strongly dependent on the grain volume distribution width.

In addition, it can be seen that at the two S_v levels investigated, both the coefficients are relatively insensitive to S_v: at each $\ln\sigma_g$ level, it was found that the values of both the coefficients were slightly lower for the coarser grain size. However, this appears as a second-order effect compared to the control exerted by the grain volume distribution width. Consequently, the behavior of these polycrystals can be studied fruitfully without regard to the S_v levels employed.

In order to further investigate the plastic flow characteristics of these polycrystals, their true stress at constant strain, true strain at constant stress and the work hardening at constant strain and constant stress were calculated from the Ludwig equation, using the appropriate experimental values for σ_y, K and n. Strain/stress levels used in the calculation were kept below the macroscopic uniform strain limit (i.e. the point of stress instability).

True stress at constant strain. The tensile strength of the polycrystals at a true strain level of 0.05 as a function of $\ln\sigma_g$ for S.P. and H.P. series (without regard to the S_v levels) is shown in Figure 3.17. It can be seen that while the two purities of samples fall

Table 3.5
Grain volume distribution width and the strength coefficient (K) and strength exponent (n) of H.P. $S_v(1)$ samples.

Sample	$\ln\sigma_g$	K, MPa	n
SP(1)1-1	1.21	165	0.57
SP(1)1-2	1.21	163	0.56
SP(1)2-1	1.28	158	0.54
SP(1)2-2	1.28	160	0.54
SP(1)3-1	1.35	160	0.52
SP(1)3-2	1.35	157	0.53
SP(1)4-1	1.78	153	0.49
SP(1)4-2	1.78	155	0.50
SP(1)5-1	2.23	127	0.42
SP(1)5-2	2.23	123	0.41
SP(1)6-1	2.79	110	0.41
SP(1)6-2	2.79	112	0.40

Table 3.6
Grain volume distribution width and the strength coefficient (K) and strength exponent (n) of S.P. $S_v(2)$ samples.

Sample	$\ln\sigma_g$	K, MPa	n
SP(2)1-1	1.21	166	0.55
SP(2)2-1	1.28	160	0.55
SP(2)3-1	1.35	148	0.51
SP(2)4-1	1.78	137	0.46
SP(2)5-1	2.23	117	0.41
SP(2)6-1	2.79	110	0.40

Table 3.7
Grain volume distribution width and the strength coefficient (K) and strength exponent (n) of H.P. $S_v(1)$ samples.

Sample	$\ln\sigma_g$	K, MPa	n
HP(1)1-1	1.01	213	0.61
HP(1)1-2	1.01	215	0.60
HP(1)1-3	1.01	211	0.62
HP(1)2-1	1.13	198	0.56
HP(1)2-2	1.13	200	0.58
HP(1)3-1	1.15	191	0.57
HP(1)3-2	1.15	188	0.57
HP(1)4-1*	1.17	182	0.55
HP(1)5-1*	1.22	172	0.56
HP(1)6-1	1.25	169	0.55
HP(1)6-2	1.25	166	0.55
HP(1)7-1*	1.31	163	0.54
HP(1)8-1	1.33	160	0.53
HP(1)8-2	1.33	159	0.52

Table 3.8
Grain volume distribution width and the strength coefficient (K) and strength exponent (n) of H.P. $S_v(2)$ samples.

Sample	$\ln\sigma_g$	K, MPa	n
HP(2)1-1	1.01	208	0.60
HP(2)2-1	1.13	196	0.55
HP(2)3-1	1.15	181	0.54
HP(2)4-1	1.17	180	0.54
HP(2)5-1	1.22	169	0.52
HP(2)6-1	1.25	166	0.50
HP(2)7-1	1.31	160	0.50
HP(2)8-1	1.33	155	0.50

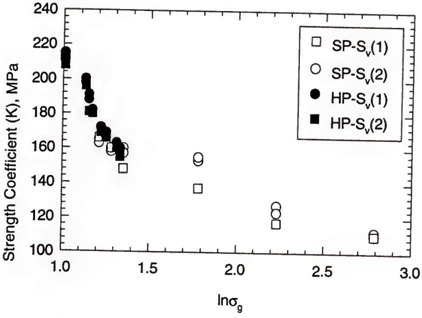

Figure 3.15 Strength coefficient from the modified Hollomon equation as a function of the grain volume distribution width.

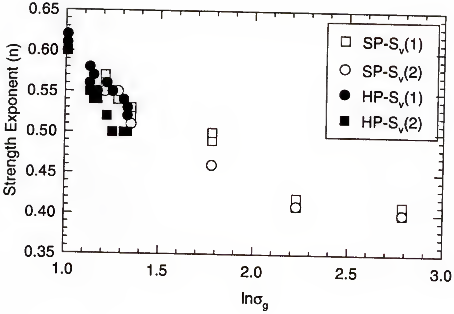

Figure 3.16 Strength exponent from the modified Hollomon equation as a function of the grain volume distribution width.

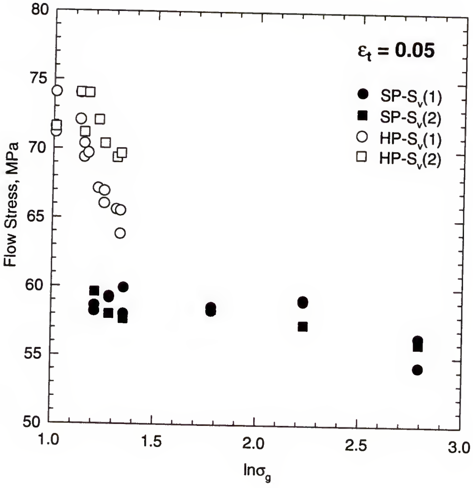

Figure 3.17 Flow stress at a true strain of 0.05 as a function of the grain volume distribution width for S.P. and H.P. purities and two S_v levels.

in two distinct groups, there is no clear distinction due to the S_v. Similar behavior was also observed at other strain levels (not shown). Consequently, the data for the two purities could be compared without any special distinction based on the S_v levels. The tensile strength at constant strain (ε_t = 0.05, 0.1, 0.2 and 0.3) for S.P. and H.P., when plotted as a function of $(\ln\sigma_g)^{-2}$ show a linear dependence, Figures 3.18(a) and 3.18(b), respectively.

Similar to the yield behavior, if the intercepts are taken as the intrinsic matrix strength with increasing deformation content, an interesting trend is observed: the intrinsic strength increases with increasing strain, however, the difference in the intrinsic strengths of the two purities of aluminum disappears at higher strains, Figure 3.19(a). The figure also shows a typical power-law type stress-strain behavior, as seen clearly by the strong linear dependence of $\log(\sigma_t)$ on $\log(\varepsilon_t)$, Figure 3.19(b). Based on Figure 3.19(b), the power law for the intrinsic matrix can be represented as follows:

$$\sigma_{(i)} = \sigma_{y(i)} + K_i \varepsilon_{t(i)}^{n_i} \tag{3.28}$$

where the subscript "i" denotes intrinsic property, with the strength coefficient and exponent being 124.7 MPa and 0.27, respectively. Note that these data are derived from the dependence of the tensile strength on a global microstructural parameter. Consequently, the values do not represent the properties of a single crystal in any particular orientation; rather, the special stress equilibrium/strain compatibility constraints placed on the deforming grains in a polycrystal are reflected in these values,

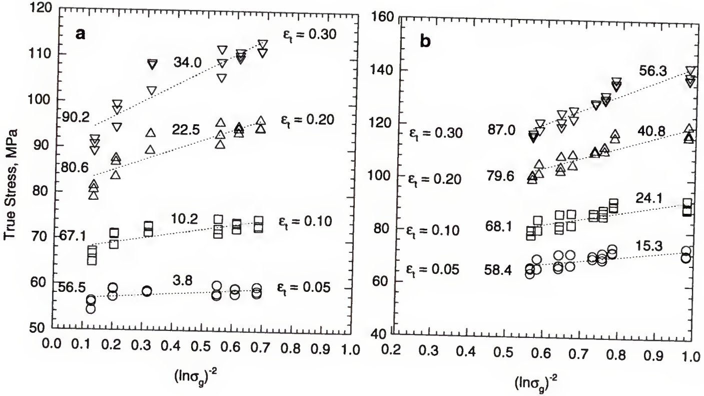

Figure 3.18 Flow stress at true strains ranging from 0.05 to 0.3 as a function of the inverse square of the grain volume distribution width illustrating the stress lag with increasing $\ln\sigma_g$. No distinction made on the basis of the S_v levels. (a) S.P. and (b) H.P.

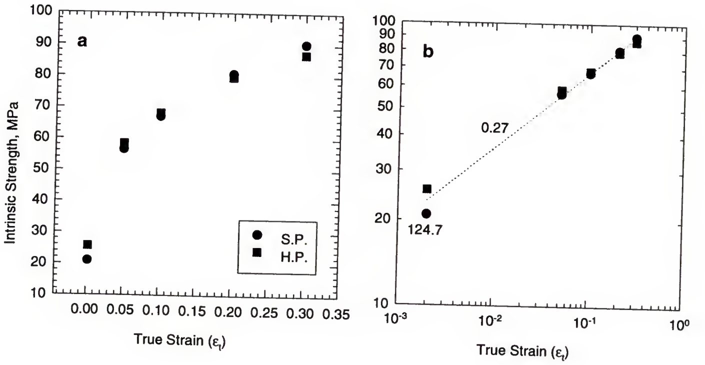

Figure 3.19 Intrinsic strength of S.P. and H.P. purities derived on the basis of σ_t vs $(\ln\sigma_g)^{-2}$ at constant strain. (a) Shows the intrisic flow curve and (b) Linear dependence on a $\log(\sigma_t)$-$\log(\varepsilon_t)$ plot indicating power law type behavior.

albeit without the grain boundaries. In other words, a flow curve based on these parameters must represent an "average grain" in an idealized polycrystal comprised of grains of equal volume.

As indicated earlier, the slopes may be taken as the sensitivity of the polycrystals to changes in the distribution width. The present data show that this sensitivity increases with increasing deformation level. Prima facie, this may appear to be contradictory since it is well known that the effect of grain boundaries decreases with increasing deformation. In particular for aluminum, high plastic deformation leads to a polygonization of the substructure and stable dislocation cell arrangements. Consequently, the observation that with increasing strain, the effect of $\ln\sigma_g$ does not diminish, but in fact increases may be attributed to the strain distribution in the early stages of plasticity and therefore to the starting microstructural state. It may be hypothesized that strain gradients on the scale of grain size increase rather than decrease in importance as the overall deformation increases, particularly for special instances where large grains may be located on the free surface of the tensile specimen. This idea is developed further in the next chapter.

True strain at constant stress. A plot of true strain at constant stress reveals another aspect of the dependence of polycrystal deformation on GVD width, Figures 3.20(a) and 3.20(b), for S.P. and H.P. series, respectively. The figures shows true strain as a function of GVD width at true stresses of 50, 75, 100 and 125 MPa. It can be seen that at lower stress regimes (< 75 MPa), the strains exhibit a linear dependence on the grain volume distribution width. However, a deviation from linearity becomes more

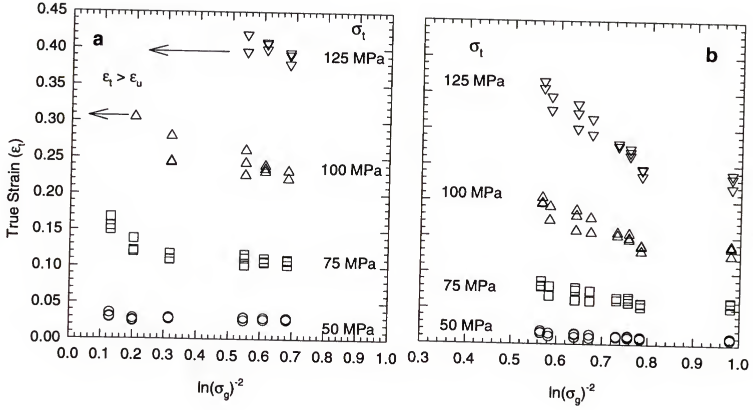

Figure 3.20 True strain at constant stress as a function of the inverse square of the grain volume distribution width illustrating the strain lag with decreasing $\ln\sigma_g$. Arrows indicate strain greater than the macroscopic uniform strain limit. (A) S.P. series and (b) H.P. series.

noticeable at a true stress of 75 MPa. Also, while the difference in the two purities is not striking, the higher purity material nevertheless exhibits a greater deformation at comparable stress and $\ln\sigma_g$ levels.

Referring to Figure 3.20(a), it should be noted that at the high stress levels, the higher distribution widths are not included because their strain levels exceeded the macroscopic uniform strain limit. Another, more subtle aspect of the data shown here is the increasing amount of scatter with increasing stress: such scatter may indicate stress (and strain) localization at higher stresses, i.e. early stages of neck development. This observation is consistent with data presented in the last section, and is developed further later in this chapter.

Work Hardening at Constant Strain. Using the Ludwig equation, the work hardening is defined meaningfully upto the uniform strain limit as:

$$\left.\frac{d\sigma_t}{d\varepsilon_t}\right|_{\varepsilon_y \le \varepsilon_t \le \varepsilon_u} = K \cdot n \cdot \varepsilon_t^{n-1} \qquad (3.29)$$

where "t" denotes true stress/strain, "y" denotes yield (offset) strain and "u" denotes uniform strain. The other quantities are as defined before. The work hardening calculated on the basis of equation 3.29 for a true strain of 0.05 is shown as a function of the grain volume distribution width in Figure 3.21. The data are plotted without distinguishing between either the two purities or the two S_v levels. It can be seen that the

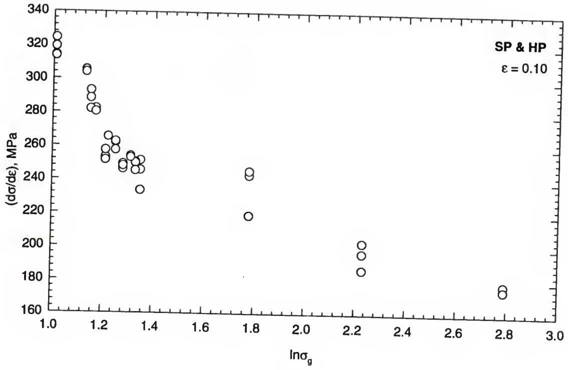

Figure 3.21 Work hardening in S.P. and H.P. purity polycrystals as a function of the grain volume distribution width at a true strain of 0.10. Data shown without distinction on the basis of Sv.

work hardening decreases monotonically with increasing distribution width. The data, plotted in the manner of the Y.S. data, i.e. *vs* $(\ln\sigma_g)^{-2}$ for ε_t of 0.05, 0.1, 0.2 and 0.3 show a strong linear dependence, Figure 3.22. It can be seen that in each case the linear correlation is maintained, but with a decreasing intercept and slope.

Following the earlier discussion, if the intercepts are taken as a measure of the intrinsic matrix work hardening, it can be seen that the work hardening decreases with increasing strain, which is consistent with the distribution dependence of flow stress.

The slope of these plots gives a measure of the control exerted by the grain volume distribution width on the polycrystal work hardening. Taken together, the behavior at all strains (less than the uniform strain limit) indicates that at small strains, polycrystals with more uniform grain volumes (narrow distribution widths) work harden more than those which contain a greater variation of grain volumes. At higher strains, the difference between the work hardening of these polycrystals diminishes. The change in the intrinsic matrix strength (intercept) and distribution ($\ln\sigma_g$) dependence (slope) as a function of the true strain is summarized in Figure 3.23.

A comparison of the intrinsic work hardening derived from two different procedures can now be made in order to check for the self-consistency of the data as well as the validity of the analysis procedures employed.

It may be recalled that the intrinsic matrix strengths were derived from plots of σ_t *vs* $(\ln\sigma_g)^{-2}$ at various true strain levels; the intercepts of the plots being the intrinsic matrix strengths, Figure 3.19(a).

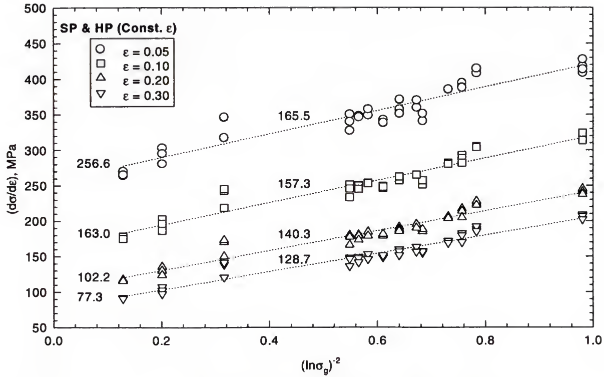

Figure 3.22 Work hardening as a function of the inverse square of the grain volume distribution width. Data for S.P. and H.P. purities plotted without distinction on the basis of Sv level. Illustrates a decrease in work hardening as well as distribution width dependence with increasing strain.

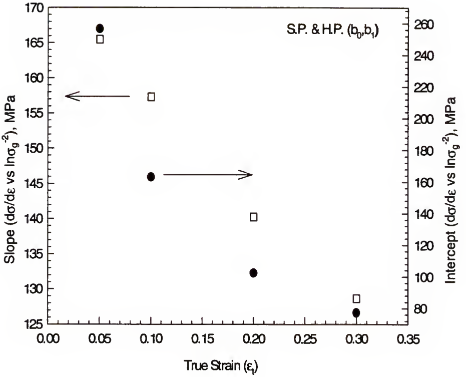

Figure 3.23 Distribution dependence of work hardening (slope) and intrinsic matrix work hardening (intercept) as function of true strain. Illustrates the decreasing influence of grain volume distribution width on work hardening with increasing strain (decreasing slope) and intrinsic matrix power-law flow behavior.

Using equation 3.26 and the K and n values, the work hardening was calculated as a function of true strain and compared with the values summarized in Figure 3.23. The comparison is shown in Figure 3.24. It can be seen that the values calculated from the two different procedures compare very well, indicating a good self consistency in the data as well as ensuring that no propagating errors are introduced during the analysis.

The above data point to a very interesting and hitherto unsuspected aspect of microstructure-dependent work hardening. For single phase polycrystals, it is well known that the work hardening rate is dependent on (i) the test temperature, (ii) the strain rate, (iii) the strain level, (iv) the impurity content and (v) the average grain size. In the present investigation, when the work hardening rate is compared at constant strain and purity level, all of the above factors are constant. Despite this, significant differences are observed in the work hardening rate. Consequently, it is clear that it the single remaining factor, i.e. the grain volume distribution is the controlling factor.

As discussed in greater detail in the next chapter, this aspect of polycrystal deformation can not be explained unless the concept of inhomogeneity of plastic deformation is invoked [48Boa, 81Rhi, 83Gok]. This concept is based on the observation that, on a macroscopic scale, grains of differing volumes deform to differing extents. As a direct consequence, one can visualize the manner in which some parts of the polycrystal remain relatively undeformed until later stages of plasticity. Briefly, it can be hypothesized that those grains which are bounded by a high amount of surface area per unit volume (i.e. the finer "size classes" of the volume distribution) require a greater

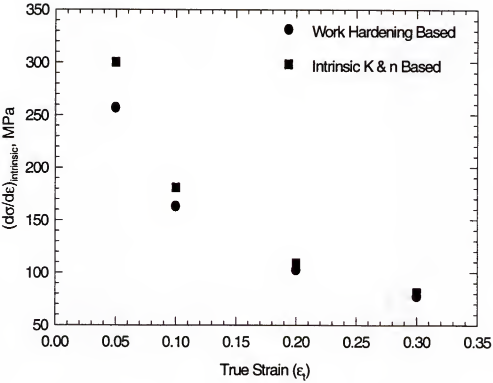

Figure 3.24 Comparison of intrinsic work hardening calculated based on work hardening at constant strain vs $(\ln\sigma_g)^{-2}$ relationship and the work hardening at constant strain calculated from intrinsic values of the strength coefficient and exponent.

expenditure of energy and are therefore initially bypassed, while for the coarser grains (i.e. those with a lower surface area per unit volume) an exact opposite situation prevails.

As a result, the progress of deformation in the polycrystal can be thought of as a continuum of response states in which each state on the average corresponds to participation of those grains which offer the least resistance *and* produce the necessary macroscopic shape change. Note that although a grain may initially have a lower grain boundary area per unit volume and therefore deform preferentially, the local work hardening must increase its resistance to deformation until it equals that of those which have been bypassed, corresponding to the next state in the continuum.

It can be seen that this hypothesis not only conforms to the overall polycrystal work hardening behavior, but also explains the differences in the work hardening rates of the samples tested in this investigation. This idea is developed in more detail in the next chapter, along with microstructure-based calculations and the important tie-in with a distribution-modified Hall-Petch type analysis.

Work Hardening at Constant Stress. Using the Ludwig equation, the work hardening as a function of stress is defined upto the uniform strain limit as:

$$\left.\frac{d\sigma_t}{d\varepsilon_t}\right|_{\sigma_y \le \sigma_t \le \sigma_u} = K \cdot n \cdot \left\{\frac{\sigma_t - \sigma_y}{K}\right\}^{\frac{n-1}{n}} \tag{3.30}$$

where σ_u is the true stress upto the uniform strain limit and other quantities are as defined before. The relation was obtained by differentiating the Ludwig equation with respect to true strain and substituting for true strain to obtain the stress dependence of the work hardening. It can be seen that at a true strain corresponding to the yield strength (0.002 in this investigation), the work hardening is zero.

The work hardening at constant stress as a function of $(\ln\sigma_g)^{-2}$ is shown in Figure 3.25. Calculations indicated that no clear separation existed based on either the purity or the S_v level. Consequently, the data for both series and S_v levels were treated as a single set, and plotted at four stress levels: 50, 75, 100 and 125 MPa. It can be seen that there is a considerable scatter at the higher stress levels, while the data appear to intermingle at the two lower stress levels employed in the calculation. The overall polycrystal flow behavior is of course also reflected in these plots, with the work hardening decreasing at increasing stress levels. Another point to be noted is the absence of data at the higher distribution widths. This is because at the stress levels used in this calculation, the uniform strain of some of the samples was exceeded; these samples are not included in this plot.

The data show clearly that the effect of the grain volume distribution persists into the late stages of plastic deformation. However, at high stress (and strain) levels in the polycrystal, it is difficult to imagine that the grain volumes (and their differences) can have any significant control over deformation mechanisms. This is especially so in view of the fact that all the grains in the polycrystal must contain high dislocation densities and a more or less stable (and uniform) dislocation cell distribution [73Fuj]. Consequently, it

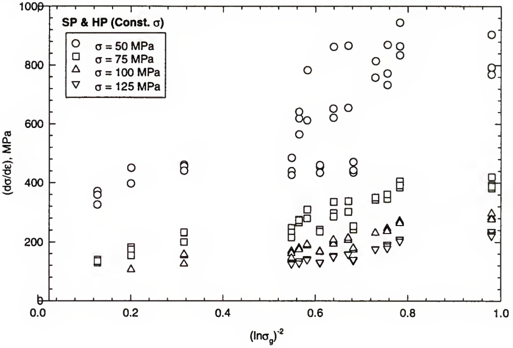

Figure 3.25 Work hardening at constant stress as a function of the inverse square of the grain volume distribution width. Data for both S.P. and H.P. purities plotted without distinction on the basis of S_V level. Illustrates the weak linear dependence of constant-stress work hardening and a decreasing separation of the data at different stress levels with increasing stress.

must be concluded that the deformation history of individual grains plays a significant role, manifesting in an apparent GVD effect at high strains. For example, comparison of work hardening behavior of polycrystals with narrow and high distribution widths shows that at constant stress, the narrow GVD width polycrystals always lag in strain. As discussed in greater detail in the next chapter, one can consider the statistical probability (as a function of the GVD width) of larger grains encountering the free (outer) surface of the tensile specimen. Coupled with this probability, if one now considers strain localization in these grains from the early plastic stages, it is possible to visualize the manner in which they can exert a control over the later stages of plastic response. As discussed below, the GVD appears to affect both the uniform and fracture strain, again pointing to a distribution-dependent strain localization.

3.2.2.3 Stress at Instability, Maximum Uniform Strain and Fracture Strain

During plastic deformation under uniaxial tensile load, the increase in stress due to reduction in the cross sectional area is initially balanced by the increase in the matrix strength due to work hardening. For aluminum, observation of the sample during plastic flow shows significant surface roughening due to local, inhomogeneous shape changes of the surface grains. It can be assumed that, during continued flow, one or more of these surface sites eventually gives rise to a higher-than-average reduction in the area of cross section, thus reducing the (local) stress required for continued deformation.

Such a situation is autocatalytic in that the higher the localized area change, the higher the stress concentration, leading to ever greater strain localization. Such a strain localization generally culminates into formation of a macroscopic neck, which is in effect a mild notch. This stage of plastic flow is commonly termed as tensile instability because the stress state in the sample changes from purely axial to triaxial (axial, radial and transverse) and the external load required to continue the deformation (at the externally imposed cross-head velocity) decreases. Thus the point of tensile instability also corresponds to the (macroscopically) uniform strain limit.

As noted before, the flow conditions for the point of tensile instability can be calculated from the flow curve by using Considere's analysis. A derivation of the governing equation relating the macroscopic uniform strain limit to flow constants is straightforward, as given below. The subscripts "o" and "i" denote the original, instantaneous values and t denotes the true stress and strain.

Since the external load decreases upon macroscopic strain localization, the instability condition can be written as:

$$P_{instability} = P_{\max} \tag{3.31}$$

Thus for the instantaneous value of the load,

$$dP_i = 0$$

Since the load is related to the true stress by

$$
\begin{aligned}
P_i &= \sigma_t A_i \\
dP_i &= A_i d\sigma_t + \sigma_t dA_i \\
&= 0
\end{aligned}
$$

and

$$
-\frac{dA_i}{A_i} = \frac{d\sigma_t}{\sigma_t} \tag{3.32}
$$

From the volume constancy during deformation relationship,

$$
\begin{aligned}
A_0 L_0 &= A_i L_i \\
d(A_0 L_0) &= d(A_i L_i) \\
&= 0
\end{aligned}
$$

and

$$
-\frac{dA_i}{A_i} = \frac{dL_i}{L_i}
$$

substituting in equation (3.29),

$$
\frac{d\sigma_t}{\sigma_t} = \frac{dL_i}{L_i}
$$

the r.h.s. in the above equation can be replaced by the derivative of the true strain since,

$$
\begin{aligned}
\varepsilon_t &= \ln(1+e) \\
d\varepsilon_t &= \frac{dL_i}{L_i}
\end{aligned}
$$

Thus,

$$
\frac{d\sigma_t}{d\varepsilon_t} = \sigma_t \tag{3.33}
$$

Substituting in equation (3.30) for the work hardening and the flow stress from the constitutive flow equation (i.e. the modified Hollomon equation), thus,

$$\sigma_t = \sigma_y + k_h \varepsilon_t^{n_h}$$

and

$$\frac{d\sigma_t}{d\varepsilon_t} = k_h n_h \varepsilon_t^{n_h - 1}$$

we arrive at the governing equation for the uniform strain calculation as,

$$\frac{\sigma_y}{k_h} = n_h \cdot \varepsilon_u^{n_h - 1} - \varepsilon_u^{n_h} \tag{3.34}$$

where σ_y is the yield strength, k_h and n_h are the strength coefficient and exponent from the Hollomon equation, respectively, and ε_u is the maximum true uniform strain. Using equation 3.34, the maximum uniform strain (ε_u) can be easily calculated by using a Newton-Raphson type iteration procedure. The calculated ε_u values can then be substituted in the Ludwig equation to obtain the corresponding tensile stress at instability (σ_u). The values of ε_u and σ_u calculated in this manner are plotted as function of the grain volume distribution width, Figures 3.26 and 3.27, respectively.

The changes in sample lengths after fracture are illustrated pictorially in Figure 3.28. The samples shown were chosen as representative of each $\ln\sigma_g$ level, regardless of the average S_v value, and range from a true strain of 0.76 to 0.57.

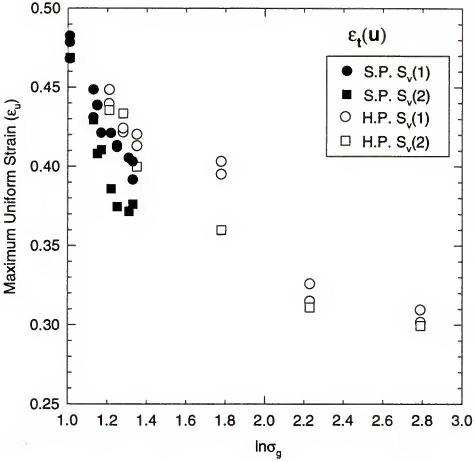

Figure 3.26 Uniform strain as function of the grain volume distribution width illustrating a monotonic decrease in the uniform strain with increasing $\ln\sigma_g$. . Data for both S.P. and H.P. purities and S_v levels.

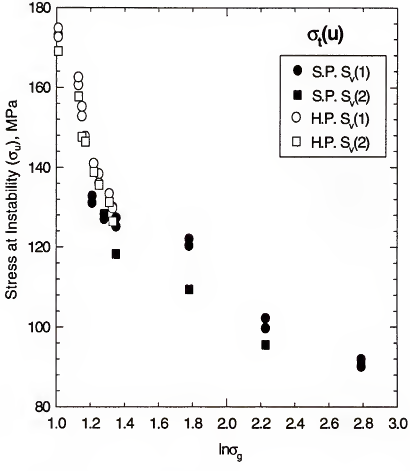

Figure 3.27 The stress at the point of tensile instability (macroscopic neck formation) as a function of the grain volume distribution width. Data for both S.P. and H.P. purities and S_v levels.

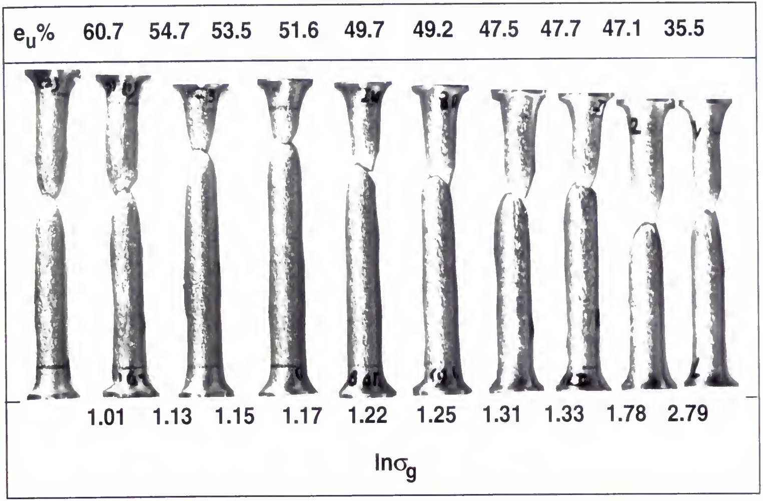

Figure 3.28 Pictorial view of change in sample lengths after fracture with the grain volume distribution width decreasing from left to right. The values of uniform strain are listed on top. Representative samples shown for each grain volume distribution width.

It can be seen that the uniform strain as well as the stress at the point of tensile instability decrease monotonically with increasing GVD width. It thus appears that the magnitude of the stress at instability and the maximum uniform strain are intimately tied to the manner in which the plastic flow is controlled by the grain volume distribution.

An attempt was also made to determine the true fracture strain, which is defined as $\varepsilon_f = \ln(A_0/A_f)$, where A_o and A_f are the original and final areas of cross section. However, the final area of cross section has to be measured in the plane of fracture. In the present experiments, a unique plane of fracture could not be defined with any reasonable accuracy. Consequently, the areas, which were measured by digitizing SEM micrographs were deemed to be inaccurate, and therefore could not be used to establish a reliable trend.

CHAPTER 4

DISCUSSION

The data presented in chapter 3 show clearly that all aspects of tensile deformation of high purity aluminum polycrystals are affected by the grain volume distribution width. In the discussion which follows, the plastic response of polycrystals is examined in relation to stress and strain distributions on the scale of grain size, effects arising from spatial arrangement of grains and spatial distribution of grain boundary areas in the test specimens, probabilities of larger-than-average grain/free surface encounters and the increase in volume domination by large grains with increasing grain volume distribution width. Microstructure-based flow stress calculations along with supplementary experimental evidence are also presented, which clearly suggest that a global microstructural characterization must be included in the general theoretical and experimental treatments of the plastic deformation of single phase polycrystals.

4.1 Progression of Plastic Deformation in Polycrystals

For simplicity, the onset and progression of plastic deformation in polycrystals may be subdivided as follows:

(a) Establishment of a stress concentration pattern, predominantly at grain boundaries due to elastic incompatibility between adjacent grains.

(b) Onset of microyielding at grain boundaries and establishment of a network of "geometrically necessary" dislocations closely mimicking the grain boundary network. Relaxation of plastic incompatibility and establishment of a grain size "feedback" system.

(c) Onset of macroyielding, with a preponderance of sites at the external (free) surface.

(d) Propagation of deformation in the bulk, with the deformation pathways selected on the basis of system feedback in (b).

(e) Establishment of "statistically stored" dislocation population in deformed regions, selective strain hardening and switching of deformation pathways. Increase in the flow stress and high initial work hardening rate.

(f) Continued switching of deformation pathways, deformation propagation through the entire cross section, establishment of stable dislocation cell structure and a continuous decrease in the work hardening rate.

(g) Strain localization at free surface sites, particularly at large grains, leading to initial stages of neck formation.

(h) Continued strain localization leading to macroscopic neck formation, void coalescence and fracture.

The discussion which follows is subdivided into three main sections: (i) the macroyield regime, (ii) strain hardening and (iii) macroscopic neck formation and fracture.

4.2 Microyield

4.2.1 Elastic Incompatibility

Consider an isotropic polycrystal under the action of an external load. While such a polycrystal is characterized by a random distribution of grain orientations and is thus macroscopically isotropic, the individual grains in the aggregate nevertheless exhibit elastic anisotropy characteristic of their crystal symmetry [67Hoo]. Meyers and Ashworth [82Mey] showed that for a crystal system with cubic symmetry, the difference in the Young's modulus in different crystallographic directions can be dramatic: for Ni, for example, the Young's modulus in the [111] direction is more than twice as high as in the [100] direction. Consequently, under the same applied stress, a [100] grain would undergo approximately twice the strain as a [111] grain, if there were no interfacial constraints. However, because of the strain compatibility constraint along grain surfaces, incompatibility stresses are created. Following Hirth's analysis [72Hir], the stresses due to such interfacial constraints can be divided into two components: longitudinal and shear, as defined in the simplified example in Figure 4.1. Calculations by [82Mey] further show that the interfacial shear stress in the longitudinal direction can be as high as three times the homogeneous shear stress on the grain interiors.

4.2.2 Onset of Microyielding

A combination of the resolved shear stress at the grain boundaries and the shear stress concentration due to elastic incompatibility cause plastic deformation in the grain boundary regions of the polycrystal. Such deformation may be termed as microyielding because it does not penetrate into the grain interiors due to cross slip caused by the orientation differences between the resolved shear stress and the stresses generated by the elastic incompatibility. As a consequence, this stage of plastic deformation establishes a dislocation network in the polycrystal which closely follows the grain boundary network without regard to the grain size. Following Ashby [70Ash], this dislocation population may be termed as "geometrically necessary" because it relaxes the elastic incompatibility between neighboring grains.

While microyielding must occur without any grain size effect, with increasing strain[1] we can expect the resulting long range stress fields to be modulated on the scale of the grain size, as illustrated in Figure 4.2. *The polycrystal may now be viewed as a system in which a mechanism exists for sensing the entire grain volume distribution.* Using this concept, an important connection is established between the macroscopic deformation of a polycrystal and the microscopic selection of deformation pathways.

---

[1] It may noted that because of the constant crosshead velocity technique commonly used in tensile tests (present investigation included), the strain is externally imposed and the stress states follow.

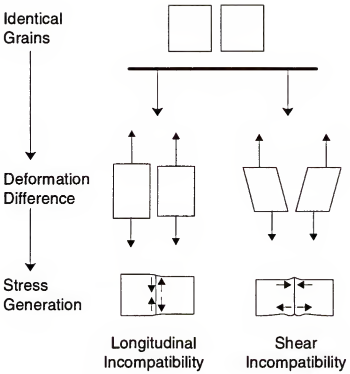

Figure 4.1 The generation of elastic incompatibility stresses in initial stages of polycrystal deformation [82Mey].

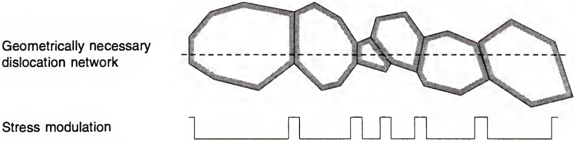

Figure 4.2 Generation of geometrically necessary dislocations and modulation of a long-range stress field due to work hardening near grain boundaries.

4.3 Macroyielding

The stage at which plastic deformation propagates into the grain interiors may termed as macroyielding. In the context of the present investigation, the key question to be answered concerns the distribution of deformation in the polycrystal. As a starting point, if the deformation path is assumed to be completely non-selective, the strain in each grain in the polycrystal must equal the macroscopic strain. This is clearly unrealistic and not supported by any experimental evidence. On the other hand, if it is assumed that the deformation begins in the large grains, i.e. selection on the basis of grain volumes, the effect of the grain volume distribution can be included in the general formalism, as discussed below.

Support for the selection of deformation path on the basis of grain volumes is provided by Taylor-limit relaxation calculations by Kocks and Canova [81Koc]. They addressed the question of how many slip systems would be required to deform grains in a polycrystal and concluded that the Taylor limit (requirement of at least five slip systems to produce any arbitrary strain) may be relaxed for less constrained regions. Thus, for example, a non-surface equiaxed grain in a polycrystal would require all five slip systems at some edges and corners, three to four systems at the bounding surfaces and two to three systems in the center, as shown schematically in Figure 4.3. While the exact number of slip systems activated must depend on the geometric and crystallographic details at the local level, it is nevertheless expected that in any given volume element, the number of slip systems will decrease with decreasing constraints. Because the stresses needed to

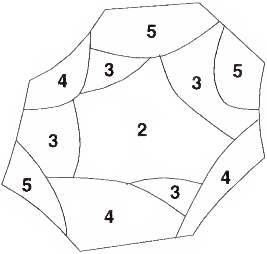

Figure 4.3 Schematic representation of slip systems activated in an equiaxed grain in a polycrystal. Based on [81Koc]. Shows decrease in slip systems away from edges and corners.

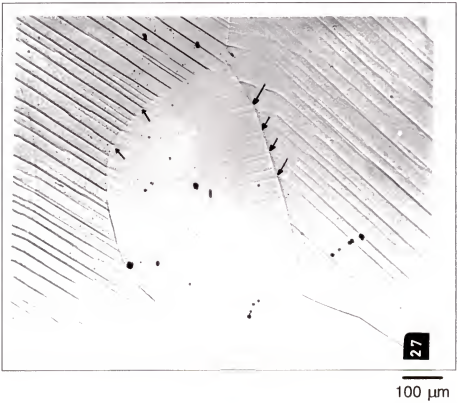

Figure 4.4 Slip line pattern in surface grains illustrating selective bypass of a small grain. Grain size distinction based on boundary curvature.

activate a certain plastic state decrease with decreasing number of slip systems [81Koc], a lowering of the flow stress may be expected in the effective Taylor-limit stress with strain. It should be noted, however, that the relaxation of constraints holds over only a part of the volume and the additional local adjustments that are necessary must always raise the flow stress [70Ash].

From the above discussion, it is clear that the lowering of the flow stress from its Taylor limit value must be a function of the fraction of unconstrained volume, which is directly a function of the grain volume.[2] Thus, we can expect the "apparent flow stress" of a grain in a polycrystal to be inversely related to its volume. In global terms, an isotropic polycrystal can then be said to exhibit an apparent flow stress distribution which closely follows and is inversely related to the grain volume distribution. Under conditions of prescribed (externally imposed) strain, the plastic deformation will propagate via paths of least resistance, i.e. predominantly through the largest grains in the principal strain directions. While this does not exclude all other grains from the deformation process, it does imply that the largest grains are predisposed to deform first.

As described in the last chapter, there are many instances in the literature where strain gradients on the scale of grain size have been reported. In the present investigation, slip line examination of surface grains revealed instances where small grains were deformed only to the extent of shear accommodation at the grain boundaries, while the larger surrounding grains showed extensive deformation, as illustrated qualitatively by the micrograph in Figure 4.4. It may be noted that a distinction in the relative sizes (grain volumes) of the grains was not made based on the sizes seen on the two dimensional cross section, but rather on the basis of boundary curvatures. Thus the bounding surfaces of the smaller grain are convex outward with respect to its volume.

---

[2] The relaxation of constraints is directly related to the closeness of the volume element to grain surfaces, edges and corners. Consequently, the lower the grain boundary area per unit volume for an individual grain, the higher will be the fraction of volume which is unconstrained. In general, the grain boundary area per unit volume is inversely related to the volume. For regular shapes, for example, $\frac{S}{V}=k\sum_i \frac{1}{x_i}$, where k is a constant and x_i's are the characteristic dimensions used.

Additional evidence for selective grain deformation is provided by utilizing the experimental procedure[3] described in the last chapter for grain-by-grain transmission Laue analysis. The x-ray patterns for three grains weighing 63.6, 5 and 1 mg are shown in Figures 4.5(a) to 4.5(c), receptively. Qualitatively, it is clear that the larger grain shows greater deformation. Note that due to the transmission Laue technique utilized, the loss in x-ray intensity (and therefore an underestimation of the amount of deformation) is greater, the larger the grain size.

4.3.1 Connection to the grain volume distribution

As outlined above, both a mechanism for grain size feedback and an inverse relation between the distribution of flow stresses and the grain size (volume) distribution has been established. Consequently, a formal connection between the grain volume distribution and the plastic response of polycrystals can now be established.

Assume that a Hall-Petch type mechanism is operative for the deformation of individual grains in the polycrystal, whether based on the dislocation pile-up model or on the dislocation forest density approach. However, instead of using an average value of

---

[3] HP series polycrystalline aluminum sample annealed at 600 °C for 4 hours, compressed 8% at 77 K, followed by grain separation at 50 °C. Separated grains cleaned and subjected to x-ray analysis.

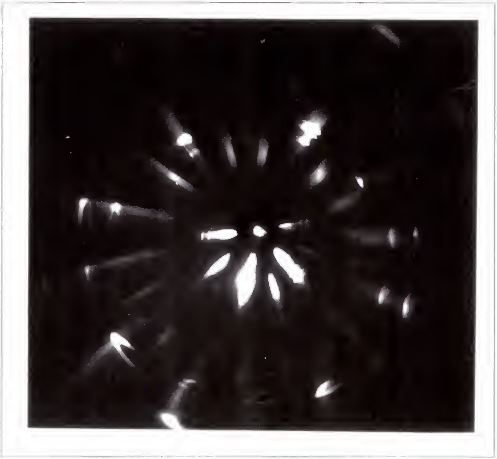

Figure 4.5 The transmission Laue x-ray diffraction patterns for a grains separated from a sample deformed 8% in compression at 77 K. Shows evidence of varying deformation content based on the amount of asterism present. (a) grain weight of 63.6 mg, (b) grain weight of 5 mg and (c) grain weight of 1 mg.

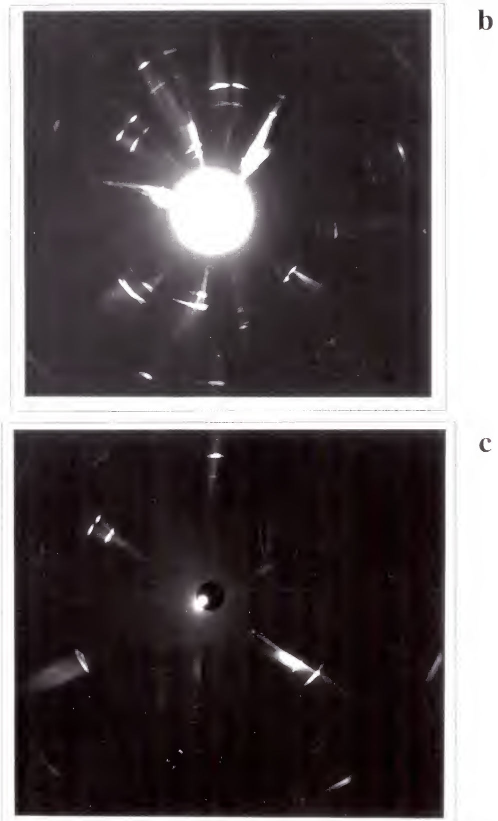

Figure 4.5 (continued).

the "grain size" (grain boundary area per unit volume) for the polycrystal as a whole, the averaging can be carried out on the basis of the grain volume distribution parameters. Note that such an averaging implicitly takes into account the increasing control of flow stress by the larger grains with increasing grain volume distribution width.

For the averaging calculation, the following steps were used:

(i) assume that for each grain size, the Hall-Petch relation holds, thus,

$$\sigma(x) = \sigma_0 + k_p x^{-\frac{1}{2}} \tag{4.1}$$

where $\sigma(x)$ is the yield strength of grains of size "x", σ_0 is the intrinsic matrix strength and k_p is the so-called Petch slope.

(ii) multiply the flow stress of each size class with its volume fraction in the distribution, and

(iii) calculate the average of the multiplication.

The governing equation for the yield strength calculation can then be written as:

$$\sigma_y = \int_{x_{min}}^{x_{max}} \sigma(x) \frac{x^3 f(x)}{\int_{x_{min}}^{x_{max}} x^3 f(x) dx} dx \tag{4.2}$$

where *f(x)* is the lognormal grain size distribution function given by:

$$f(x) = \frac{1}{\sqrt{2\pi}\ln\sigma_g} \frac{1}{x} \exp\left[-\frac{1}{2} \left(\frac{\ln x - \ln \mu_g}{\ln \sigma_g} \right)^2 \right] \tag{4.3}$$

where σ_g and μ_g are the geometric standard deviation and mean of the equivalent diameter distribution, respectively.

Constants. the value of σ_0 was taken to be 25.62 MPa, i.e. the intrinsic matrix strength of H.P. purity aluminum determined in chapter 3. The k_p value on the other hand is not available from the experimental data in the present investigation. Consequently, it was calculated using equation 4.2 and the yield strength and grain size distribution parameters of one sample. A sample with the lowest distribution width (1.01) was chosen for the purpose, which yielded a value of 0.521 $\text{MPa}\bullet\text{mm}^{1/2}$. The integration limits were based on the experimentally determined size distributions.

Equation 4.2 was integrated numerically. The results of the calculation along with the experimental yield strengths as a function of the inverse square of the grain volume distribution width are shown in Figure 4.6. It can be seen that the calculated values not only show the same trend but also the magnitudes are close to the experimental values. While the good correlation between the experimental and calculated yield strengths lends credence to the mechanistic basis of the calculations, the approximately linear dependence of yield strength on the inverse square of the distribution width cannot be explained using similar arguments. Consequently, such a dependence must be considered as purely empirical at this time.

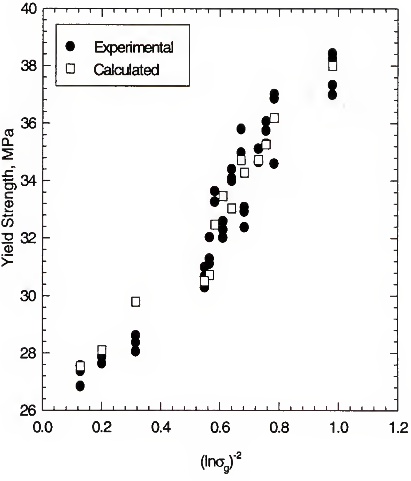

Figure 4.6 Comparison of experimental and calculated values of yield strength as a function of the grain volume distribution width. The experimental data modified as indicated in Figure 3.13. Calculation based on grain volume distribution modified Hall-Petch.

4.4 Strain Hardening

With increasing strain beyond macroyield, the apparent flow stress distribution must change due to strain hardening at the grain size level. This is because the apparent flow stress of a deforming grain, which was initially controlled by its volume, will now have the added contribution from local work hardening. As a first approximation, it may be hypothesized that as soon as the net apparent flow stress of grains of a particular volume equals that of the next size, the deformation must spread in those grains also. The consequence of this view of the deformation process is that the slope of the stress-strain curve ($d\sigma/d\varepsilon$) is controlled not only by the local work hardening but also by the increasing amount of grain boundary area participating in the deformation process. For aluminum in particular, the work hardening decreases continuously as a function of strain. This suggests that the fraction of grains participating in the deformation process must increase very rapidly below true strains of 0.1 or so. The rate of activation of additional grain boundaries must nevertheless be controlled by the spread in grain sizes, i.e. the grain volume distribution width. One further consequence of such selection of deformation paths is that at a comparable macrostrain, the polycrystal with a narrow distribution width (denoted by P_n) will exhibit a higher flow stress compared to one with a wider distribution width (denoted by P_w). In other words, P_n will always "lead" P_w in stress at comparable strains and always "lag" in strain at comparable stress, which is consistent with the experimental data presented in chapter 3.

It may appear rather surprising that differences in grain volumes alone would exert such a degree of control over the strain hardening behavior. Indeed, the more common representations of distribution data (as a frequency curve or cumulative frequency on a probability scale) do not effectively illustrate the increasingly dramatic differences in grain volumes in polycrystals with increasing grain volume distribution widths. A volume-based analysis on the other hand does reveal these differences well. One may, for example, calculate the percentage of total volume occupied by a given percentage of grains by number (denoted by $V_v(N\%)$), starting with the largest grains in the distribution. The results of such a calculation are presented in Figure 4.7. It can be seen that the volume domination by a small number of large grains increases dramatically with increasing distribution width: for example, comparison of the two limits of the distribution widths in this investigation show that for an $\ln\sigma_g$ of 1.01, $V_v(5\%) = 20.5\%$, while for an $\ln\sigma_g$ of 2.78, $V_v(5\%) = 67.8\%$. The increase in volume domination not only affects the initial apparent flow stress distribution, but also must increase the probability of large grain /large grain contacts. Such contacts are likely to further decrease the flow stress due to a decrease in the deformation path resistance.

The experimental σ_t-ε_t curves indicate that even at high strains, the grain volume distribution effect persists. The observation can not be explained simply on the basis of grain selection, since all grains in the polycrystal must be participating in the process, and especially since all the polycrystals contained (nominally) the same average grain boundary area per unit volume. Clearly, other processes such as preferential section

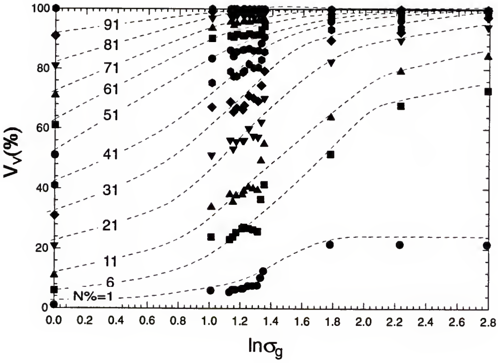

Figure 4.7 Volume based calculations illustrating the domination of total volume by the largest grains in the distribution.. The data show the fraction of total volume occupied by number% of grains as a function of the grain volume distribution width. The calculations are carried out starting with the largest grains in the distribution.

reductions at sites of intersections of large grains with the external "free" surface of the specimen must intervene.[4]

4.5 Neck Formation

It was shown in chapter 3 that the maximum macroscopic uniform strain is a monotonically decreasing function of the grain volume distribution width. The site(s) at the external surface at which necking may initiate may be thought of as being biased toward local microstructural geometry, machining defects..etc. Assuming that the distribution of machining defect sites is indistinguishable from sample to sample, one may turn towards the probability of shear thinning at the local level. In fact, it has been proposed [85Rhi] that the necking sites are selected early in the deformation process, based on the local microstructural scale. If the probability of grain encounters with the external surface is examined, it can be shown that the probability scales with the caliper diameter of the grains [94Deh]. In other words, there is a greater probability of encountering a grain on the random external surface, the larger its volume.[5]

Using the volume domination arguments presented in the last section, it is clear that two additive effects are present with increasing $\ln\sigma_g$: (i) an increased probability of encountering an especially large grain on the free surface and (ii) the volume of the largest grains is greater. In the presence of these effects as well as reduced geometrical constraints due to the free surface and the size of the grains, it is certainly likely that the localized shear thinning originates at the large grains on the external surface. To some extent, the process is autocatalytic since, once initiated, the macroscopic stress at the cross section must increase, leading to a further concentration of deformation.

---

[4] It is also possible that the historical (in terms of macroscopic stress) "lag" in the deformation of P_w-type polycrystals can not be entirely overcome at larger strains before necking processes take over. Also, there may exist effects related to a correlation between the crystallographic orientation of a grain and its size. However, such correlations have not been established at the present time.

[5] For the same reason, there is always an overestimation of the number of large grains on a random 2-d section through a 3-d polycrystal. Conversely, the small grains are underestimated since they appear with a frequency less than in the volume.

Consistent with the experimental data, the arguments based on grain encounter probability clearly suggest that increasing the grain volume distribution width must increase the probability of a macroscopic neck formation earlier in the strain history, i.e. a lowering of the maximum macroscopic uniform strain.

CHAPTER 5

CONCLUSIONS AND FUTURE WORK

5.1 Conclusions

This work has established, for the first time through direct and unambiguous experimental techniques, that all aspects of the plastic response of single phase polycrystal are affected by the dispersion in grain volumes. This represents the single most important conclusion of the present work. In addition the details of grain volume dispersion in single phase polycrystals and the control of polycrystal mechanical behavior are as follows:

(i) The grain volume distribution in high purity aluminum polycrystals was consistently well approximated by the lognormal function.

(ii) The width of the lognormal distribution function was the single most important parameter for establishing correlations between the dispersion of grain volumes and mechanical behavior of the polycrystals.

(iii) The width could be controlled systematically by controlling the thermomechanical processing history of the samples, and decreased monotonically in a power law manner with increasing severity of deformation prior to recrystallization. In addition, the evolution of the width was dependent not only on the absolute but also on the relative severity of each deformation step, provided that a recrystallization treatment was given between the steps.

(iv) The yield strength, flow stress at constant strain and the work hardening rate showed a strong linear dependence on the inverse square of the grain volume distribution width. All these properties as well as the maximum uniform elongation decreased monotonically with increasing width.

(v) Within the limits tested, the average grain boundary area per unit volume (4.45 and 8 mm^2/mm^3) did not significantly alter the plastic response.

(vi) A new view of plastic deformation of single phase polycrystals was presented, which takes into account stress and strain distributions on the scale of grain size, effects arising from spatial arrangement of grains and spatial distribution of grain boundary areas in the test specimens, probabilities of larger-than-average grain/free surface encounters and an increase in volume domination by large grains with increasing grain volume distribution width.

(viii) The yield strengths of the polycrystals could be predicted by assuming that the Hall-Petch mechanism was active for each grain in the polycrystal, while the overall plastic response was dependent on grain volume distribution based averaging.

5.2 Future Work

One of the important aspects of polycrystalline microstructures not addressed in the present work is the crystallographic orientation distribution function. In particular, no information is currently available regarding any connections between the grain volume and the orientation distribution (GVD and ODF) functions. Since both aspects of polycrystalline microstructures have a profound impact on their mechanical behavior, a fundamental metallurgical investigation to elucidate their evolution during thermomechanical processing would be of practical as well as theoretical interest.

Such an investigation will significantly increase our understanding of the underpinnings of global microstructural evolution in single phase polycrystals and their plastic response. As such, the study may provide a capability to simultaneously predict the GVD and ODF parameters, a more detailed understanding of the recrystallization process and, equally importantly, a capability to carry out more realistic global microstructure/orientation based mechanical property calculations.

REFERENCES

[1879McA] D. McAlister, *Proc. Roy. Soc.,* (**29**), p.367 (1879).

[03Kap] J.C. Kapteyn, *Skew Frequency Curves in Biology and Statistics,* Publ.: Noordhoff, Groningen, (1903).

[19Des] C. Desch, *J. Inst. of Metals,* (**22**), p.241 (1919).

[22Lin] J.W. Lindeberg, *Math. Z.,* (**15**), p.211 (1922).

[25Lev] P. Levy, *Calcul des Probabilities,* Publ.: Gauthier-Villars, Paris, (1925).

[29Hat] T. Hatch and H. P. Choate, *J. Franklin Inst.,* (**207**), p.369 (1929).

[31Sch] E. Schmidt, *Z.Elektrochem.,* (**37**), p.447 (1931)

[33Dav] G.R. Davies and W.F. Crowder, *Methods of Statistical Analysis in Social Sciences,* p.301, Publ.: J. Wiley and Sons, New York, (1933).

[38Tay] G.I. Taylor, *J.Inst.Metals,* (**62**), p.307 (1938)

[44Hal] P.R. Halmos, *Ann. Math. Statist.,* (**15**), p.182 (1944).

[45And] W.A. Anderson and R.F. Mehl, *Trans. AIME,* (**161**), p.140 (1945).

[45Hol] J.H. Hollomon, *Trans. AIME,* (**162**), p. 268 (1945)

[45Kal] M. Kalecki, *Econometrica,* (**13**), p.161 (1945).

[46Dav] G.R. Davies, *Econometrica,* (**14**), p.219 (1946).

[47Eps] B. Epstein, *J. Franklin Inst.,* (**224**), p.471 (1947).

[48Boa] W. Boas and M.E. Hargreaves, *Proc.Royal Soc. Series [A],* (193), p. 89 (1948)

[48Dal] J.M. Dallavalle, *Micrometrics,* Chapter 5, 2nd Ed., Publ.: Pitman, New York, NY (1948).

[48Smi] C.S. Smith, *Trans. AIME,* (**175**), p.15 (1948).

[49Day] B.B. Day, *Rev. Inst. Int. Statist.,* (**17**), p.129 (1949).

[50Bec] P.A. Beck and P.R. Sperry, *J. Appl. Phys.,* (**21**), p.150, (1950).

[50Kot] F. Kottler, *J. Franklin Institute,* (**250**), p. 339 (1950).

[51Bis] J.F.W. Bishop and R. Hill, *Phil Mag.,* (**42**), p.414,1298 (1951)

[51Esh] J.D. Eshelby, F.C. Frank and F.R.N. Nabarro, *Phil.Mag,* (**42**), p.351 (1951)

[51Hal] E.O. Hall, *Proc.Phys.Soc. London,* (**B64**), p.747 (1951)

[52Wil] W.M. Williams and C.S. Smith, *Trans. AIME,* (**194**), p.755 (1952).

[53Car] R.P. Carreker and W.R. Hibbard, *Acta.Met.,* (**1**), p.654 (1953)

[53Pet] N.J. Petch, *J.Iron Steel Institute,* (**174**), p.25 (1953)

[57Car1] R.P. Carrekar, Jr., and W.R. Hibbard, Jr., *Trans. AIME,* **209(10)**, p.1157 (1957).

[57Car2] R.P. Carreker, *Trans. AIME,* (**209**), p.112 (1957)

[57Fel] P. Feltham, *Acta. Met.,* (**5**), p.97 (1957).

[57Iak] E.S. Iakoleva, Fiz.Met. Metalloved., **4(1)**, p. 145-150 (1957).

[57Tro] T.A. Trozera, O.D. Sherby and J.E. Dorn, *Trans. ASM,* (**49**), p. 173 (1957)

[58Bal] W.M. Baldwin, Jr., *Acta. Met.,* (**6**), p. 139, (1958)

[58Cot] A.H. Cottrell, *Trans. TMS AIME,* (**212**), p.192 (1958)

[58Koc] U.F. Kocks, *Acta. Met.,* (**6**), p. 85, (1958)

[59Ric] Li.T. Richards and S.F. Pugh, *J. Inst. of Metals,* (**88**), p.399 (1959).

[60Bai] J.F. Bailey, *Phil. Mag.,* (**5**), p.833, (1960).

[60Hos] W.F. Hosford, R.L. Fleischer and W.A. Backofen, *Act.Met.,* (**8**), p.187 (1960)

[60Ros] W. Rostoker, J.M. McCaughey, and H. Markus, *Embrittlement by Liquid Metals,* Publ.: Reinhold, New York, NY (1960).

[61How] S. Howe and C. Elbaum, *Phil.Mag.,* **61(6)**, p.37 (1961)

[61Sui] J.C. Suits and B. Chalmers, *Acta.Met.,* (**9**), 854 (1961)

[62Joh] A.A. Johnson, *Phil.Mag.,* (**7**), p.177 (1962)

[62Keh] A.S. Keh, *Direct Observation of Imperfection in Crystals,* p.213, Newkirk and Wernick (Ed.), Interscience, New York (1962)

[63Con1] H. Conrad, *Electron Microscopy and Strength of Crystals,* p.299, T.Washurn (Ed.), Interscience, New York (1963)

[63Con2] H. Conrad, *Acta.Met.,* (**11**), p.75 (1963)

[63Con3] H. Conrad and B. Christ, *Recovery and Recrystallization of Metals,* p.124, L. Himmel (Ed.), Interscience, New York (1963)

[63Hig] W.I. Higuchi and E.N. Hiestand, *J. Pharm. Sci.,* (**52**), p.67 (1963).

[63Hor] E. Hornbogen, *Trans.ASM,* (**56**), p.16 (1963)

[63Li] J.C.M. Li, *Trans.TMS-AIME,* (**227**), p.247 (1963)

[63Mea] J.D. Meakin and N.J. Petch, *ASD-TDR-63-324,* p.243, Orlando, FL. (1963)

[63Pos] S.N. Postlethwait, *First Int. Congress for Stereology,* (**37a/1**), Publ.: Congress Print, Vienna, (1963).

[63Wei] S. Weissmann, T. Imura, and N. Hosakawa, *Recovery and Recrystallization of Metals,* p.241, Ed.: L. Himmel, Publ.:Interscience, New York., (1963).

[63Wil] D.V. Wilson and J.A. Chapman, *Phil.Mag.,* (**8**), p.1543 (1963)

[64Deh] R.T. DeHoff, *Trans. Met. Soc. AIME*, (**230**), p.764 (1964)

[64Hul] F. Hultgren, *Trans. Met. Soc. AIME*, (**230**), p. 898 (1964)

[64Smi] E. Smith and P.J. Worthington, *Phil.Mag.*, (**9**), p.211 (1964)

[64Wor] P.J. Worthington and E. Smith, *Acta.Met.*, (**12**), p.1277 (1964)

[65Bun] H.J. Bunge, *Z.Metallkde.*, (**56**), p.872 (1965)

[65Car] W.E. Carrington and D. McLean, *Acta.Met.*, (**13**), p.493 (1965)

[65Dye] L.D. Dyer, *Trans. ASM*, (**68**), p.620 (1965).

[65Hop] R.A. Hopkins and R.W. Craft, *Trans. AIME*, (**233**), p.1526 (1965).

[65Mar] M.J. Marcinkowski and R.M. Fisher, *Trans.TMS-AIME*, (**233**), p.293 (1965)

[65Roe] R.J. Roe, *J.Appl.Phys.*, (**36**), p.2024 (1965)

[66Cho] Y.T. Chou, *J.Appl.Phys.*, (**37**), p.2425 (1966)

[67Cho] Y.T. Chou, *J.Appl.Phys.*, (**38**), p.2080 (1967)

[67Con] H. Conrad, S. Feuerstein and L. Rice, *Mater.Sci.Eng.*, (2), p.135, (1967)

[67Hoo] R.E. Hook and J.P. Hirth, *Acta. Met.*, (**9**), p. 191 (1967)

[67Li] J.C.M. Li and J.C.T. Liu, *Phil.Mag.*, (**15**), p.1059 (1967)

[68Deh] R.T. DeHoff, *Quantitative Microscopy*, p.307, R.T. DeHoff and F.N. Rhines (Ed.), McGraw-Hill, New York, (1968)

[68Ess] U. Essman, M. Rapp and M. Wilkins, *Acta. Met.*, (**16**), p. 1275 (1968)

[68Hen] J.H. Hensler, *J. Inst. Metals*, (**96**), p.190 (1968).

[68Hir] J.P. Hirth and J. Lothe, *Theory of Dislocations*, p.701, McGraw-Hill, New York, (1968)

[68Kau] J.G. Kaung and T. Mura, *J.Appl.Phys.*, (**39**), p.109 (1968)

[68Sch]	F. Schuckher, *Quantitative Microscopy,* p. 207, R.T. DeHoff and F.N. Rhines (Ed.), Publ.: McGraw-Hill, New York, (1968)
[69Chi]	G.Y. Chin and W.L. Mammel, *Trans.TMS-AIME,* (**245**), p.1211 (1969)
[69Han1]	N. Hansen, *Trans. Met. Soc. AIME,* (**245**), p. 1305 (1969)
[69Han2]	N. Hansen, *Trans. Met. Soc. AIME,* (**245**), p. 2061 (1969)
[70Koc]	U.F. Kocks, *Met.Trans.,* (**1**), p.1121 (1970)
[70Li]	J.C.M. Li and Y.T. Chou, *Met.Trans.,* (**1**), p.1145 (1970)
[71Abr]	H. Abrams, *Metallography,* (**54**), p.59 (1971).
[72Con]	R.G. Connell, Jr., *Ph.D. Dissertation,* University of Florida, Gainesville, FL (1972).
[72Hir]	J.P. Hirth, *Met. Trans.,* (**3**), p. 3047 (1972)
[72Oka]	K. Okazaki and H. Conrad, *Met. Trans.,* (**3**), p. 2411 (1972)
[72Ota]	M. Otala and S. Saynajakangas, *J. Phys. E. Sci. Instr.,* (**5**), p.669 (1972).
[73Ait]	J. Aitchison and J.A.C. Brown, *The Lognormal Distribution,* Cambridge University Press (1973).
[73Dou]	R.M. Douthwaite and J.T. Evans, *Acta. Met.,* (**21**), p. 525 (1973)
[73Fuj]	H. Fujita and T. Tabata, *Acta. Met.,* (**21**), p. 355 (1973)
[73Ree]	R.E. Reed-Hill, *Physical Metallurgy Principles,* (2nd Edition), p. 827, Publ.: D. Van Nostrand Co., New York, (1972)
[73Tho]	A.W. Thompson and M.I. Baskes, *Phil. Mag.,* (**28**), p. 301 (1973)
[74Gar]	A.M. Garde and R.E. Reed-Hill, *STP 551,* Publ.: ASTM, p. 75 (1974)
[74Mas]	H. Masui and H. Takechi, *Trans. ISIJ,* (**16**), p. 20 (1974)
[74Mor]	M. Moravec, J. Kurdman, and P. Chraska, *Pract. Metallog.,* (**11**), p.276, 1974.

[74Ota] M. Otala, *Prak. Metallogr.,* **(11)**, p.83 (1974).

[74Rhi] F.N. Rhines and K.R. Craig, with appendix by R.T. DeHoff, *Met. Trans.,* **(5)**, p. 413 (1974).

[75Eig] E.H. Eigeltinger and R.T. DeHoff, *Met. Trans. A,* **(6A)**, p.1853 (1975).

[75Kle] J. Klee, *Ph.D. Dissertation*, Warsaw Technical University (1975).

[76Gra] C.G. Granqvist and R.A. Buhrman, *J. Appl. Phys.,* **(47)**, p.2201 (1976).

[76Joy] W.b. Joyce, R.W. Dixon and R.L. Hartman, *Appl. Phys. Lett.,* **(28)**, p.684 (1976).

[76Rhi] F.N. Rhines, K.R. Craig, and D.A. Rousse, *Met. Trans. A,* **(76A)**, p.1729 (1976).

[77Han] N. Hansen, *Acta. Met.*, **(25)**, p. 863 (1977)

[78Kre] A. Kreisler and R.D. Doherty, *Metal Science,* p.551, (Dec. 1978).

[78Pat] B.R. Patterson, *Ph.D. Dissertation,* University of Florida, Gainesville, FL (1978).

[79Gan] P. Ganesan, K. Okazaki, and H. Conrad, *Met. Trans. A,* **(10A)**, p.1021 (1979).

[80Ell] R.A. Ellis, Jr., *Ph.D. Dissertation,* University of Florida (1980)

[80Fra] V. Franetoric, M. Stubicar, and A. Bonefacic, *J. Mat. Sci.,* **(15)**, p.353 (1980).

[80Sko] O.J. Skog, *Brit. J. Addict.,* **(75)**, p.169 (1980).

[81Gho] A.K. Ghosh and R. Raj, *Acta. Met.,* **(29)**, p. 607 (1981)

[81Koc] U.F. Kocks and G.R. Canova, *Deformation of Polycrystals: Mechanisms and Microstructures (Proc. Symp.),* Second Riso International Symposium on Metallurgy and Materials Science, Riso, Denmark, 14-18 September, p. 1 (1981).

[81Rhi] F.N. Rhines, R.A. Ellis and A.B. Gokhale, *Scripta Met.,* **(15)**, p. 783 (1981)

[81Wyr] J.W. Wyrzykowski, *Ph.D. Dissertation*, Warsaw Technical University (1981)

[82Mey] M.A. Mayers and E. Ashworth, *Phil. Mag. A,* **46(5)**, p. 737 (1982)

[82Rhi1] F.N. Rhines and A.B. Gokhale, *Liquid Metal Induced Embrittlement of Metals (Proc. Symp.),* Publ.: AIME, St. Louis, MO, (1982).

[82Rhi2] F.N. Rhines and B.R. Patterson, *Met. Trans. A,* (**13A**), p.985 (1982).

[82Rhi2] F.N. Rhines, B.R. Patterson, H.H. Ho and P.J. Lasky, *Grain Refinement in Castings and Welds (Proc. Symp.),* p. 117, Ed.: G.J. Abbaschian and S.A. David, TMS-AIME Fall Meeting, St. Louis, MO, October 25-26 (1982).

[83Alh] J.T. Al-Haidary, N.J. Petch and E.R. De Los Rios, *Phil. Mag. A*, (**47**), p. 869 (1983)

[83Gok] A.B. Gokhale and F.N. Rhines, *Microstructural Science,* Ed. R.T. DeHoff, J.D. Braun and J.L. McCall, Elsevier, (**11**), p. 3 (1983)

[83Mur] J.L. Murray, *Bulletin of Alloy Phase Diagrams,* **4(2)**, p.183 (1983).

[83Wat] A.S. Watwe, *Ph.D. Dissertation,* University of Florida, Gainesville, FL (1983).

[83Wyr] J.W. Wyrzykowski and M.W. Grabski, *Metal Sci.*, (**17**), p. 445 (1983)

[84ASTM1] Specification E8, *Annual Book of ASTM Standards,* (**03.01**), p. 130, ASTM, Philadephia (1984)

[84ASTM2] Specification E238, *Annual Book of ASTM Standards,* (**03.01**), p. 394, ASTM, Philadephia (1984)

[84Liu] G.Q. Liu, *Ph.D. Dissertation,* University of Florida, Gainesville, FL (1984).

[85Die] G.E. Dieter, *ASM Metals Handbook,* (**10**), p. 20, 9th Edition, Publ.: Americal Society for Metals, Metals park, Ohio, (1985)

[86Wyr] J.W. Wyrzykowski and M.W. Grabski, *Phil. Mag. A*, **53(4)**, p. 505 (1986)

[87Pal] J.E. Palmer, C.V. Thompson and H.I. Smith, *J. Appl. Phys.,* **62(6)**, p.2492 (1987).

[90Kur] K.J. Kurzydlowski, *Scripta Met.,* (**24**), p. 879 (1990)

[92Mar] A.M. Markus, B.L. Adams and A.B. Gokhale, *Scripta Met.,* **27**(**2**), p. 155 (1992)

[93Kur] K.J. Kurzydlowski and J.J. Bucki, *Acta. Met.,* **41**(**11**), p. 3141 (1993)

BIOGRAPHICAL SKETCH

Atul Balkrishna Gokhale was born on June 11, 1953, in Poona, India. He graduated with distinction in 1976 with a Bachelor of Engineering degree in metallurgy from Poona University. After working as a metallurgical engineer for two years with Bombay Metals and Alloys, Ltd., Bombay and Kulkarni Foundries Ltd., Poona, he joined the Department of Materials Science and Engineering, University of Florida. In 1985, he completed the experimental work towards the doctoral degree under the guidance of Prof. F.N. Rhines. Since that time, he has worked on a number of areas of metallurgy and materials science, including critical evaluation and thermodynamic modeling of phase equilibria, rapid solidification processing, synthesis of high temperature composites and solidification processing in microgravity. He is joint member of TMS-AIME and a member of the Materials Research Society. He has co-authored over forty-five publications and is the recipient of two outstanding service awards from NASA.

This thesis was submitted to the Graduate Faculty of the College of Engineering and to the Graduate School and was accepted as partial fulfillment of the requirements for the degree of Doctor of Philosophy.

December, 1995

Winfred M. Phillips
Dean, College of Engineering

Karen A. Holbrook
Dean, Graduate School